

## Reviewed Preprint

v1 • March 28, 2025

Not revised

## Reviewed Preprint

v2 • April 24, 2026

Revised by authors

## ✉ For correspondence:

[Bruce.Bamber@utoledo.edu](mailto:Bruce.Bamber@utoledo.edu)

## Competing interests: No

competing interests declared

Funding: See [page 24](#)

## Reviewing editor: Andrew J King,

University of Oxford, United

Kingdom

© 2025, Saad et al. This article is distributed under the terms of the [Creative Commons Attribution License](#), which permits unrestricted use and redistribution provided that the original author and source are credited.

# Olfactory combinatorial coding supports risk-reward decision making in *C. elegans*

Md Zubayer Hossain Saad<sup>1,4</sup>, William G Ryan V<sup>2</sup>, Chelyan A Edwards<sup>1</sup>, Benjamin N Szymanski<sup>1</sup>, Lana Awa<sup>1</sup>, Jenna Kaake<sup>1</sup>, Alexander Martin<sup>1</sup>, Aryan R Marri<sup>1</sup>, Lilian G Jerow<sup>1,3</sup>, Robert McCullumsmith<sup>2</sup>, Bruce A Bamber<sup>1</sup> ✉

<sup>1</sup>Department of Molecular, Cellular, and Developmental Biology, The University of Toledo, Toledo, United States •

<sup>2</sup>Department of Neurosciences and Psychiatry, The University of Toledo, Toledo, United States • <sup>3</sup>Neuroscience Graduate Program, University of Cincinnati, Cincinnati, United States • <sup>4</sup>Department of Neuroscience, Ohio State University, Columbus, United States

## eLife Assessment

This **important** study shows that an odorant that is typically thought of as a repellent actually activates both attractant and repellent olfactory neurons in *C. elegans*.

**Convincing** evidence is provided that nematode worms can integrate signals in different sensory pathways to drive different behavioral responses to the same cue. These findings will be of interest to scientists interested in combinatorial coding in sensory systems.

<https://doi.org/10.7554/eLife.104828.2.sa4>

## Abstract

Olfactory-driven behaviors are essential for animal survival, but mechanisms for decoding olfactory inputs remain poorly understood. We have used whole-network Ca<sup>++</sup> imaging to study olfactory coding in *Caenorhabditis elegans*. We show that the odorant 1-octanol is encoded combinatorially in the periphery as both an attractant and a repellent. These inputs are integrated centrally, and their relative strengths determine the sensitivity and valence of the behavioral response through modulation of locomotory reversals and speed. The balance of these pathways also dictates the activity of the locomotory command interneurons, which control locomotory reversals. This balance serves as a regulatory node for response modulation, allowing *C. elegans* to weigh opportunities and hazards in its environment when formulating behavioral responses. Thus, an odorant can be encoded simultaneously as inputs of opposite valence, focusing attention on the integration of these inputs in determining perception, response, and plasticity.

## Introduction

Animals must detect and respond to chemical signals in the environment to find food, avoid hazards, and find mates. Olfactory systems balance two competing priorities to optimally represent the external chemical space. First, they must respond rapidly and robustly to specific compounds which elicit innate responses important for survival. These include predator or parasite odors (eliciting avoidance), and pheromones (eliciting social and/or reproductive responses) (1–4). Such stimuli are sensed using narrowly tuned odorant receptors in the periphery, hard-wired to dedicated circuits for specific behaviors (labeled line coding). Second, olfactory systems must be versatile, capable of detecting and discriminating millions of different environmental odorants. This versatility is achieved using broadly-tuned odorant receptors, which activate in different combinations depending on the chemical structure of the odorant, enabling millions of different odorants to be discriminated using, at most, a few thousand receptors (5). These combinations are decoded centrally to identify the odor (combinatorial coding)(4). Combinatorial coding has been regarded as the predominant mechanism for olfactory coding (6,

7), but examples of labeled line-like olfactory coding are increasingly being found (8–12), suggesting that olfactory coding is a hybrid of labeled line and combinatorial mechanisms (1). Labeled line coding is simpler, and probably evolved first, with animals responding to specific environmental cues using specific receptors. Combinatorial coding likely emerged later as the narrowly tuned receptor genes underwent duplication and divergence to diversify ligand binding properties. Presumably, the central decoding circuitry then evolved to take advantage of these new sources of environmental information (1, 13). The initial steps in olfactory coding are relatively well studied, with each olfactory receptor neuron expressing 1-2 olfactory receptors (14, 15). Inputs from olfactory receptor neurons expressing the same receptor converge on a single glomerulus in the olfactory bulb (mammals) or antennal lobe (insects), and the glomeruli project to higher processing centers in the brain (16). Recent studies are beginning to unravel the neural circuitry by which olfactory inputs generate perception and responses (17–20). However, we still lack a clear understanding of how combinatorial inputs are decoded, and how combinatorial pathways and labeled line pathways may functionally interact.

We have turned to *C. elegans* to study the downstream processing of olfactory inputs. The small size of the *C. elegans* nervous system and the availability of techniques for pan-neuronal activity recording now make it possible to study the neural basis for sensory-driven behaviors at whole-network scale (21–31). Olfaction in *C. elegans* has classically been viewed as a labeled-line coding system rather than a combinatorial system, where specific subsets of chemosensory neurons respond to attractive odorants and drive positive chemotaxis (AWC, AWA), or respond to repulsive odorants and drive negative chemotaxis (ASH, AWB, ADL) (32–38). However, it was recently shown that individual odorants activate multiple classes of olfactory neurons, and individual olfactory neurons respond to a wide range of odorants (39). This responsiveness profile is the hallmark of combinatorial coding, even though there are many fewer chemosensory neurons in *C. elegans*, and these neurons must express a much wider repertoire of olfactory receptors than their mammalian counterparts. The striking parallels in olfactory coding between animals as divergent as nematodes, insects, and mammals suggests that evolution may have converged on a few optimal solutions for sensing and responding to external odor landscapes (40).

We have performed an in-depth analysis of a single odorant, 1-octanol (1-oct), which is encoded combinatorially (39), and is well-known to stimulate aversive behavior (32, 33, 38, 41). We show that 1-oct stimulation concurrently activates separate attractive and repulsive sensory afferent pathways in the nervous system. These pathways converge to control at least four aspects of locomotion at the behavioral and circuit levels, with the balance between attraction and repulsion emerging as the critical factor determining the overall behavioral output. Furthermore, this coding strategy provides a simple framework for modulating sensory-driven responses to produce context-appropriate behavior.

## Results

### 1-octanol repulsion in microfluidic arenas

1-oct avoidance in *C. elegans* has been intensively studied because it is strongly modulated by nutrition state and monoamine/neuropeptide signaling cascades (34, 42–46). Our goal was to investigate the network basis of 1-oct repulsion using the NeuroPAL system (30), which allows simultaneous whole-brain  $\text{Ca}^{++}$  imaging with unambiguous neuronal identification, coupled with quantitative analysis of 1-oct aversive behavior. 1-oct has previously been utilized as a volatile stimulus (33, 34), or in a gradient on agar plates (47, 48), while NeuroPAL recordings are performed in aqueous solution in microfluidics chips under confocal microscopy (30). To better match the conditions for NeuroPAL recordings and behavioral assays, we first investigated 1-oct repulsion in microfluidics arenas (49–51), which gave us precise control over the concentration and spatiotemporal characteristics of the 1-oct stimulus. Using a simple two-chamber arena (Fig. 1A), we demonstrated that worms were repelled by a saturating concentration of 1-oct in S-basal (2.2 mM, corresponding to a  $3.75 \times 10^{-4}$  dilution; Fig. 1B–D). In our initial trials, we added 0.01% w/v xylene cyanol (0.1 mg/mL) to the 1-oct solution to visualize the interface between the

stimulus and control buffer. However, as another study reported (51), worms were significantly attracted to xylene cyanol, introducing an unwanted stimulus into the assays. We therefore optimized methods to maintain a stable interface between odorant and buffer chambers without the need for dye (see Methods). We assayed worms between 20 and 40 minutes after removal from food, during area-restricted search behavior (52), and calculated average chemotaxis indices (CIs) between 30 and 40 minutes (see Methods, and Fig. 1D, E). The  $-0.7$  CI observed in the trial shown represents strong repulsion. The average CI over  $n=5$  was  $-0.27 \pm 0.24$  (SEM).

## Network-wide response to repulsive olfactory stimulation

To investigate the neuronal basis for the observed 1-oct aversive behavior, we performed network-wide  $\text{Ca}^{++}$  imaging during 1-oct stimulation and identified the responding cells by imaging the neuronal landmarks encoded by the NeuroPAL fluorescent reporters (Fig. 2A). Worms were immobilized in ‘olfactory’ microfluidics chips (53) for microscopy. Previous whole-brain studies have shown that certain neurons undergo spontaneous transitions between low and high activity states correlating with spontaneous reversals during foraging, notably the reverse command neurons AVA, AVE, AVD, AVB, and the RIM neuron (23, 27, 54–59). We therefore used a recording/stimulus protocol consisting of a 6 min pre-stimulus period, followed by 6 30s applications of 2.2 mM 1-oct, spaced 30s apart, to help distinguish between spontaneous transitions and potential sensory-evoked transitions within this neuronal population. We observed dynamic activity patterns in dozens of neurons before and during 1-oct stimulus (Fig. 2B–D). Consistent with previous studies, AVA, along with AVE, AVD, RIM, AIB, and AIZ showed spontaneous state transitions, with the AVB forward command interneuron and the AIY interneuron showing mirror image patterns (i.e. AVB/AIY inactivated when AVA activated and vice versa). Typically, 3–4 transitions were observed in a 12 minute recording. These transitions took place during both the pre-stimulus and stimulus periods (Fig. 2D, 3A) and showed no obvious relationship with 1-oct application or withdrawal. These transitions are related to network state changes which drive spontaneous reversals during foraging in freely moving worms (60). Immobilization and anesthetization, necessary for confocal imaging, distort certain aspects of these motor command sequences compared to freely moving worms executing the motor commands and receiving proprioceptive feedback. However, the intrinsic motor programs remain intact under these conditions (60).

Sensory signals were also prominent, in both amphid and non-amphid chemosensory neurons. ASH and BAG showed strong consistent responses correlating with stimulus onset (‘ON’ responses). AWB also showed an ON response but also had high levels of spontaneous activity. ADL showed a strong ON response to the initial stimulus but was strongly desensitized in subsequent applications (Fig. 2D, 3B). ASH, AWB, and ADL were previously identified as the main neurons mediating 1-oct aversive responses (33, 34). 1-oct responses were also observed in AWA, ASE, ASK, ASJ, and URX (Fig. 2D, 3B), consistent with the observation of Lin et al, showing that 1-oct activates sensory neurons promiscuously (39). Significantly, we observed a strong 1-oct response in AWC neurons (both  $\text{AWC}^{\text{OFF}}$  and  $\text{AWC}^{\text{ON}}$ ; Fig 2D, 3B). AWC activity decreased upon 1-oct addition and rebounded upon 1-oct withdrawal, in a typical ‘OFF’ neuron pattern (61), opposite to ASH (Fig. 2B–D, 3C). This was surprising, first, because AWC is usually considered an attractive neuron, not expected to respond to a repulsive odorant, and second, because the observed AWC pattern predicts that AWC should drive attraction to 1-oct (38, 47, 61, 62). 1-oct has thus far only been described as a repellent for *C. elegans*, with no attractive properties (32, 34, 38, 48). Strong sensory-driven activity was also observed in AIA and SAA interneurons, suggesting these two neurons may receive substantial inputs from the sensory neurons (Fig. 2D, 3C). Apart from AIA, the other ‘first layer’ interneurons AIB, AIY, and AIZ did not show detectable sensory-driven activity (Fig. 3A), despite their extensive anatomical connections with sensory neurons, suggesting these interneurons may be receiving their principal functional inputs from elsewhere in the circuit.

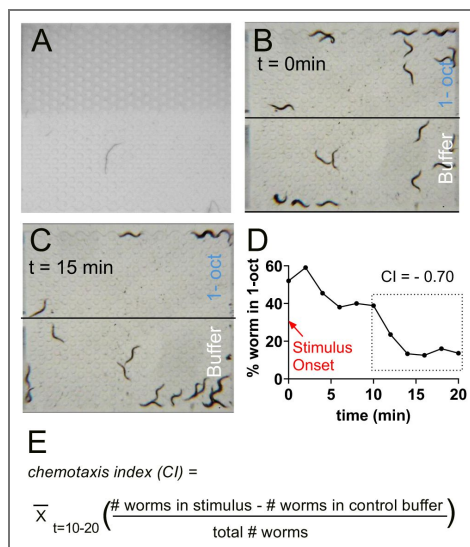


**Fig. 1. 1-oct chemotaxis in microfluidic arenas.**

(A) Microfluidics arenas were configured with two zones of equal area, one containing a 1-oct solution and the other containing buffer alone (1-oct zone contains 0.01% xylene cyanol dye for visualization here; assays are run without dye). (B, C) Typical distribution of worms when first exposed to 1-oct (B), and after 15 min of 2.2 mM 1-oct exposure (C). (D) Time-course of 1-oct chemotaxis for the trial shown in B, C (E) Calculation of chemotaxis index, averaging worm counts every 2 minutes from 10-20 minutes after introduction of 1-oct solution.



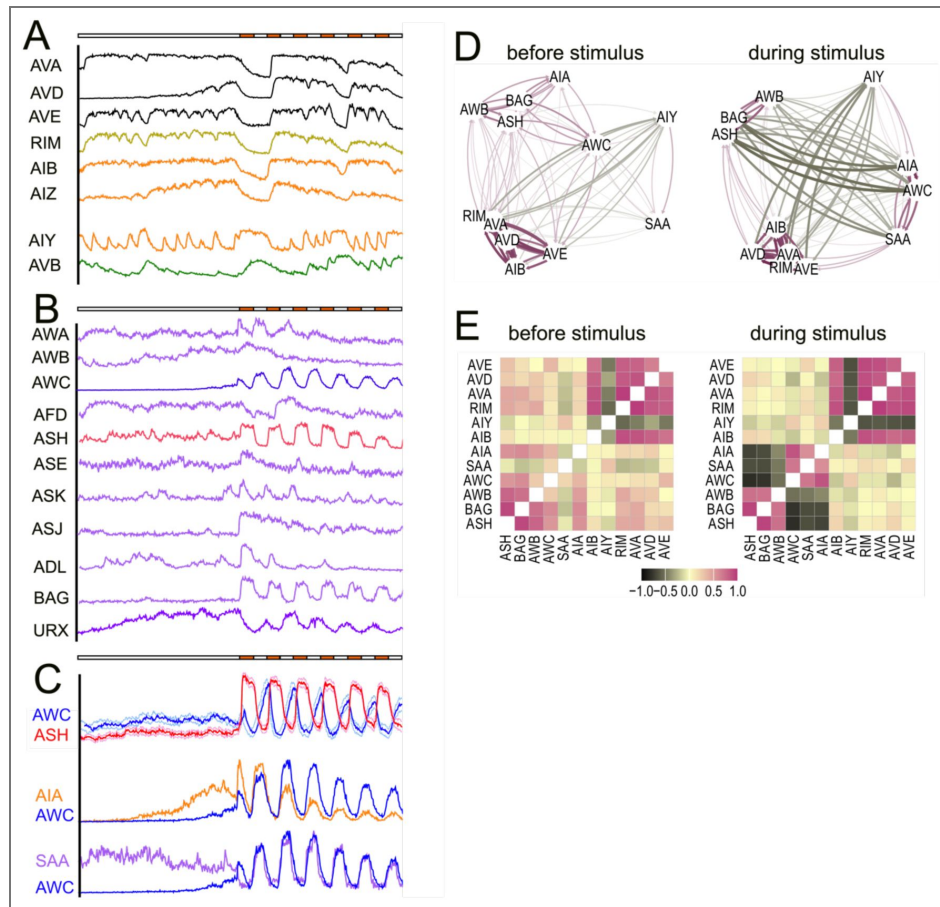


**Fig. 3. Neuronal activity correlations.**

(A-C) Neuronal activity patterns from worm shown in Fig - 2. (A) Stochastic activity state transitions of locomotory command and associated interneurons, with AIY and AVB showing opposite activity patterns to AVA, AVD, AVE, RIM, AIB, and AIZ. (B) Sensory neuron activity patterns. (C) Selected neuron pairs highlighting the anti-correlated activity patterns of AWC and ASH (top), and the correlated activity patterns of AWC with AIA (middle) and SAA (bottom). (D, E) Activity correlations for 12 selected neurons based on data from 5 worms. (D) Graph representation of activity correlations before stimulus (minutes 0-6, left) and during stimulus (minutes 6-12, right). Neurons pairs with the strongest positive correlations are closest to one another and connected by the darkest purple lines; neurons with the strongest negative correlations are furthest apart and connected by the darkest green lines. (E) Relationships from (D) presented as a correlation matrix using the same color code.

To better understand how sensory inputs may pattern global network activity patterns, we performed correlation analysis on selected data sets in which we were able to identify 12 key neurons with well characterized roles in sensory motor coupling (38, 52, 61). To detect the sensory signature, we compared neuronal correlation patterns in the first 6 minute interval (prior to stimulation), and the second 6 minute interval (where stimulus was applied and removed for alternating 30s periods) (Fig. 3D, E). We observed the expected increases and decreases in correlation among the sensory neurons (i.e. ASH and BAG became correlated, and anti-correlated with AWC). We did not observe any increased correlation between the motor command interneurons and sensory neurons, consistent with a lack of observable sensory-driven activity in the motor command interneurons. However, the degree of activity cross-correlation among AVA, AVE, AVD, AIB, and RIM increased during the stimulus period, and AIB also showed increased correlation with ASH. These observations suggest that sensory information was penetrating to the locomotory command circuit level even if there was no obvious sensory entrainment of the principal neurons in those circuits (Fig. 3D, E).

Finally, we observed several neurons with activity patterns which did not correspond to the locomotory command group or the sensory-dependent group, which included SMDV, RIA, and RMDD (Fig. 2D), which are generally associated with turning behavior (63–65).

## The balance of simultaneous repulsion and attraction shapes the chemotactic response

The observation that 1-oct application and withdrawal cycles activate ASH and AWC in alternation predicts that these two neurons generate antagonistic inputs into the locomotory circuitry. Specifically, ASH activity varies in phase with 1-oct application, predicted to stimulate in-phase reversal consistent with a repulsive chemotactic response. AWC activity varies out of phase with 1-oct application, predicted to inhibit in-phase reversals and stimulate out of phase reversals, consistent with an attractive chemotactic response. This puzzling activity pattern led us to hypothesize that 1-oct is encoded combinatorially, simultaneously as a repellent and an attractant through two distinct and opposing afferent pathways, with the balance of these pathways determining downstream events and eventual behavioral outcome.

To test this idea, we conducted several experiments to selectively inhibit the putative repulsive and attractive afferent pathways singly, with the goal of unmasking the effects of the opposite pathway. First, to selectively diminish the repulsive pathway, we reduced the 1-oct concentration. Lin et. al. reported 1-oct concentration-response relationships for the amphid sensory neurons including ASH and other neurons implicated in 1-oct avoidance (ADL, AWB), and AWC (39). At sub-saturating concentrations, the responses of ASH, and to a lesser extent AWB and ADL, showed clear concentration dependence, while the 'ON' response of AWC did not. We extended these observations to the concentration ranges we used in our behavior and imaging experiments, measuring ASH responses, and both the AWC 'ON' and 'OFF' responses, during serial stimulation of individual worms (0.22 mM, 0.66 mM, and 2.2 mM 1-oct). ASH responses showed significant concentration-dependent increases, whereas AWC 'ON' and 'OFF' responses did not (Fig. 4A-C). In parallel, we found that lower concentrations of 1-oct (0.22 and 0.66 mM) were strongly attractive (Fig. 4D), while intermediate concentrations were largely without effect (Fig. 4D). Thus, the 1-oct chemotactic response transitions from attraction, through neutral, to avoidance, as the activity of ASH (and possibly other neurons) increases relative to AWC, highlighting the potential importance of the balance of repulsive and attractive input pathways (note that 1-oct repulsion at 2.2 mM in wild type was modest and highly variable; the solubility limit of 1-oct in aqueous solution prevented testing higher concentrations). Next, we took a genetic approach using *tax-4* and *osm-9* mutations to selectively inhibit different sets of sensory neurons. TAX-4 is a cGMP-gated ion channel required for signaling in AWC and other neurons (including AWB, BAG, ASE); OSM-9 is a TRP channel which contributes to signaling in ASH and other neurons (including ADL, AWA) (38, 44, 66). Loss of TAX-4 caused 1-oct to become repulsive at all concentrations (Fig. 4E), consistent with an obligatory role for TAX-4 in the putative attractive pathway. Surprisingly, loss of OSM-9 had no significant effect on CI values at any concentration (Fig. 4E), suggesting that these

mutants may retain some residual ASH signaling (38, 67) or 1-oct repulsion may be due to multiple sensory neurons acting redundantly, some of which do not signal through OSM-9. Finally, we directly tested whether ASH and AWC, specifically, play antagonistic roles in 1-oct chemotaxis. We used chemogenetic inactivation, based on transgenic expression of *Drosophila* HisCl1 in ASH (using the *sra-6* promoter) and AWC (using the *ceh-36* promoter) (68, 69). Incubating these strains on histamine (His) results in acute, highly specific neuronal inactivation. Using 2.2 mM 1-oct as stimulus, His-minus controls were not significantly different from wild type for either the ASH-HisCl1 or the AWC-HisCl1 strain (despite the appearance of slight attraction under these specific experimental conditions). Importantly, the addition of His significantly skewed chemotaxis indices in the expected direction: CI values shifted positively for ASH HisCl1 worms (Fig. 4F) and negatively for AWC HisCl1 worms (Fig. 4G), consistent with reduced repulsive drive and reduced attractive drive, respectively. These findings strongly support the hypothesized antagonism between ASH and AWC in 1-oct chemotaxis. Overall, these three approaches provided evidence that 1-oct chemotaxis is driven by two distinct afferent input pathways with opposite valence in balance with one another, which can be distinguished by their differential concentration dependence, their differential usage of signal transduction pathways, and different primary sensory neurons providing the initial input (i.e. ASH for the repulsive pathway and AWC for the attractive pathway).

To understand the interaction of these co-activated afferent pathways at the level of locomotory decision making, we closely examined the behavior of worms as they encountered the interface between 1-oct solution and control buffer in microfluidic devices. We performed this analysis using the microfluidics 'stripe' chip (50, 51), which contains a central zone of 2.2 mM 1-oct flanked by zones containing control buffer. We used automated tracking (70) to quantify behavior upon encountering zone boundaries (i.e. reversals vs successful transits; Fig. 5A, B). For worms entering the 1-oct zone, entry transits outnumbered entry reversals by nearly 2:1 (Fig. 5B, C), which was surprising given that the overall behavioral outcome is generally avoidance under these conditions. *osm-9* mutation further depressed entry reversals, indicating that *osm-9* dependent signaling contributes to reversal in response to 1-oct in the microfluidic environment. Interestingly, *tax-4* loss-of-function strongly stimulated entry reversals, indicating that *tax-4* signaling normally suppresses these reversals, consistent with a role promoting 1-oct attraction (Fig. 5B, C). This attraction-promoting activity was also observed for worms exiting the 1-oct zone (Fig. 5B, C). Here, exit reversals strongly outnumber exit transits but in *tax-4*, the pattern is reversed, with transits outnumbering reversals by roughly 4:1. *osm-9* loss of function had no effect on exit reversals (Fig. 5C). These observations confirm that TAX-4 mediated attractive signaling significantly shapes the behavioral response to 1-oct, even though 1-oct is traditionally viewed as a strong repellent. Most importantly, they identify a locomotory transition important for chemotaxis (i.e. entry reversal frequency) in which two antagonistic sensory afferent pathways converge at a single point in time and space (Fig. 5B).

These findings were largely recapitulated by the chemogenetic inactivation of ASH and AWC. We analyzed reversal behavior at the 1-oct/buffer interface in the HisCl1 experiments shown in Fig. 4E and 4F (performed in the smaller two-chamber microfluidics arenas) (71). Inactivation of ASH had no significant effect on locomotory decision-making. However, these datasets contained very few entry reversals to begin with, so we were unable to assess the role of ASH in these events. Exit reversals were also unaffected, similar to *osm-9* trials. Importantly however, inactivation of AWC produced a very similar result to *tax-4* mutation. Entry reversals were significantly increased and exit reversals were strongly suppressed, pointing to a key role for AWC specifically in the attractive sensory afferent pathway for 1-oct chemotaxis.

These behavioral data raised a new important question: how can wild-type worms avoid the 1-oct containing zone when their reversal decisions favor entry and retention? We had noticed that contact with 2.2 mM 1-oct caused worms to rapidly and reversibly increase their locomotory activity, suggesting an additional potential mechanism in play. To quantify this effect, we measured the average distance worms moved when we flooded the microfluidics arena with 2.2 mM 1-oct, comparing the distances traveled in a 2-minute interval in control buffer and 1-oct.

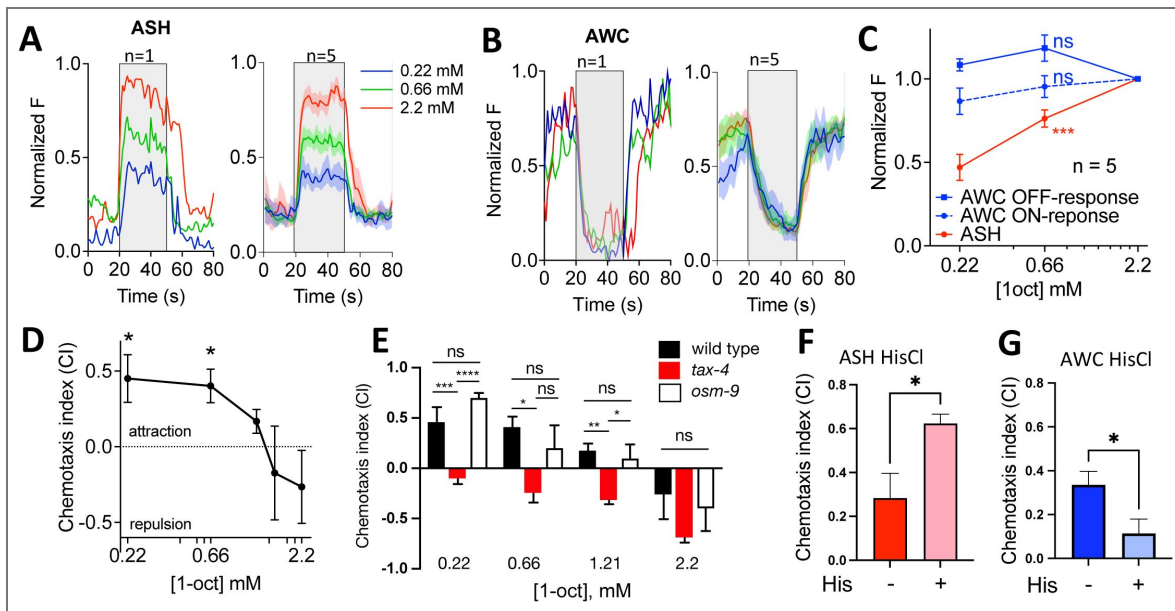


**Fig. 4. Chemotactic outcome is influenced by the balance of attractive and repulsive sensory inputs**

(A-C) ASH ON responses (A, C) are concentration dependent, while AWC ON and OFF responses (B, C) are not, over a 10-fold concentration range from 0.22 to 2.2 mM. Representative single traces (A, B, left panels), averaged traces (A, B, right panels), and concentration-response curves (C) shown; \*\*\*  $P < 0.001$ , ns  $P > 0.05$ , paired ANOVA. (D) 1-oct chemotaxis transitions from positive (attractive) to negative (repulsive) with increasing concentration; intermediate concentrations (1.21 and 1.54 mM) result in little chemotaxis; \* $P < 0.05$  compared to 2.2 mM, ANOVA. (E) *tax-4* mutants are repelled by 1-oct at all tested concentrations (\* $P < 0.05$ ; \*\* $P < 0.01$ ; \*\*\* $P < 0.005$ ; \*\*\*\* $P < 0.0005$ ; ns  $P > 0.05$ , ANOVA,  $n = 5$  for each data point). *osm-9* mutants do not differ from wild type. (F, G) chemogenetic inactivation of ASH, AWC: ASH inactivation increases the chemotaxis index, suggesting reduced repulsive drive (F); AWC inactivation decreases the chemotaxis index, suggesting reduced attractive drive (G) \* $P < 0.05$  *t*-test.

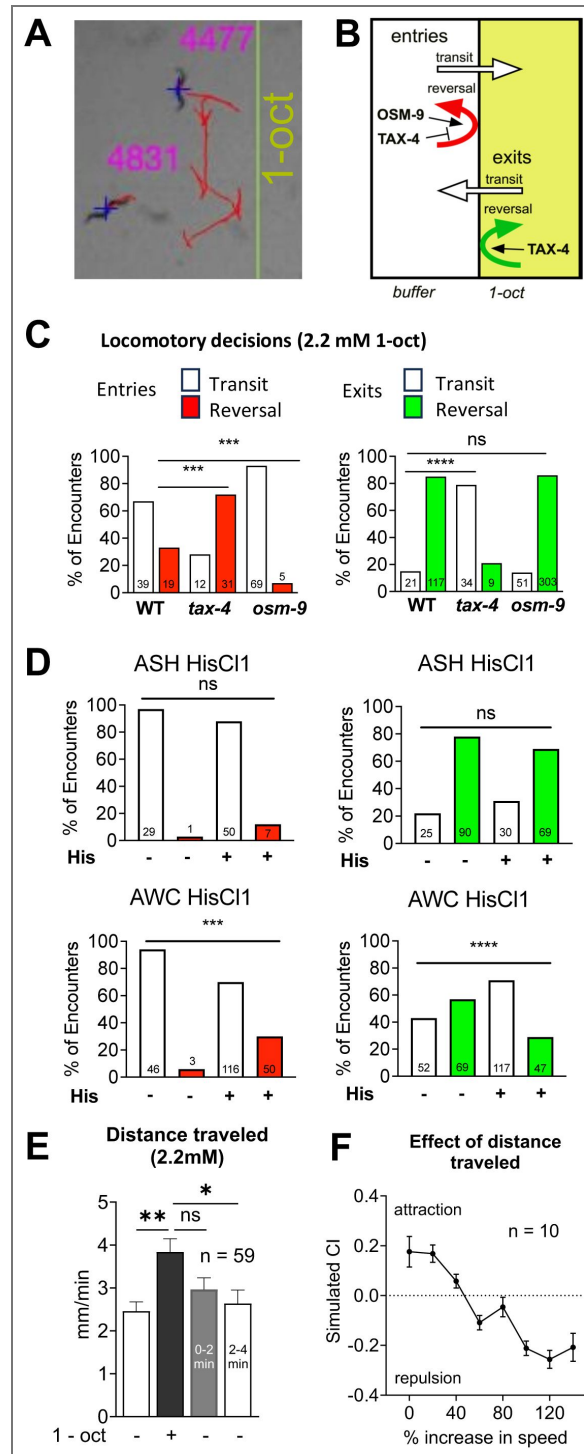


**Fig. 5. Locomotory reversals and speed modulation stimulated by 1-oct.**

(A) Example of a single worm track traced by the automated tracking software. (B) Worms execute reversals probabilistically at the 1-oct-buffer interface dependent on TAX-4 and OSM-9 signaling cascades. (C) Reversal probabilities at 1-oct-buffer interface for wild-type, *tax-4*, and *osm-9* (see panel B for summary and explanation of terms). Left panel: movement from buffer zone to 1-oct zone ('entries'). Right panel: movement from 1-oct zone to buffer zone ('exits'). (D) Reversal analysis of trials shown in 4F, G. Bars color coded as in (C). (E) Modulation of locomotory activity. Distance traveled in 2 minutes prior to, during, and after flooding the entire chip with 1-oct solution. (F) Simulation of chemotaxis outcome based on reversal probabilities (from C) and locomotory activity modulation (from E). Points shown are averages of 10 simulation trials with SEM error bars. \*\*\*, \*\*\*\* in C, D indicate  $P < 0.001$ ,  $0.0001$  Fisher's Exact Test. \*, \*\* in E indicate  $P < 0.05$ ,  $0.01$ , ANOVA (Tukey's multiple comparison test).

Worms significantly increased their locomotion in 1-oct, and returned to baseline rates 2-4 minutes after 1-oct withdrawal (Fig. 5E). Next, we created a simple behavioral simulation to determine whether this selective increase in locomotory activity could counteract the observed bias in reversal probabilities to achieve overall avoidance. The environment was modeled as a line divided into two equal compartments, representing the control buffer and the 2.2 mM 1-oct halves of the arena. Worms were modeled as one-dimensional particles, free to move along the full length of the line. They were allowed to reverse direction at random along the length of the line but were specified to reverse direction with fixed probabilities at the buffer/octanol interface, depending on which direction they approached from. Finally, the particles moved at different relative rates in the buffer and 1-oct compartments (Fig. 5F). Using our measured entry and exit reversal probabilities as inputs, this simulation showed that relative locomotory speed is a critical factor determining overall chemotaxis behavior, with a 60% speed increase sufficient to convert attraction to repulsion, given our observed interface reversal probabilities in the stripe chips (Fig. 5F). This simulation was highly simplified and did not account for the persistence of higher locomotion speeds once worms exited 1-oct (Fig. 5E), which could further potentiate repulsion since faster-moving exiting worms will be oriented away from the 1-oct zone, biasing their trajectories toward the further reaches of the buffer zone where they eventually slow. Importantly, these results extend the idea that 1-oct is encoded combinatorially, generating afferent inputs controlling at least three distinct aspects of locomotion: 1) promotion of reversals when encountering increased [1-oct], 2) promotion of reversals when encountering reduced [1-oct], and 3) increase of locomotory speed in the presence of increased [1-oct].

## Repulsive and attractive signaling competitively entrain the locomotory command neurons

To understand how the repulsive and attractive 1-oct signals affect locomotory reversals at a circuit level, we examined the activity pattern of the AVA reverse command interneuron in relation to 1-oct addition and withdrawal. First, it was necessary to develop a data analysis approach to detect and quantify sensory-driven patterns of AVA activation, given the well-documented patterns of spontaneous AVA activity state transitions (23, 27, 54–59) that could potentially obscure a sensory signal. To reduce the impact of these transitions, we averaged at least 6 recordings of AVA activity for each condition tested so that non sensory-associated AVA transitions would tend to average out with larger numbers of recordings, akin to spike-triggered averaging (72–74). We then calculated the ‘entrainment index’ (EI), as a measure of how strongly a response is positively or negatively correlated with 1-oct application, and quantified the probability that an observed correlation is greater than a random association (see Methods), setting a threshold of  $P < 0.05$  for non-random association. To validate this test, we analyzed ASH and AWC responses to 1-oct application, which were obviously highly correlated and anti-correlated, respectively. The ASH and AWC EIs showed the expected positive and negative values, with  $P < 0.0015$ , indicating a less than one in six hundred chance that the correlations in neuronal responses with 1-oct applications were random (Fig. 6A, B). Applying this test to AVA activity, we observed strong inverse correlation with stimulant application at 0.22 mM 1-oct (the lowest tested concentration), and a significant negative EI value (Fig. 6C, D, H). This concentration was attractive and showed the lowest ASH:AWC activity ratio (Fig. 4C), suggesting that AWC may be driving AVA with minimal interference from ASH. At higher [1-oct] (0.66, 2.2 mM), AVA entrainment with 1-oct application was shifted positively (compared to 0.22 mM; Fig. 6C, D, H) and was not significantly different from random ( $P > 0.05$ ). At these concentrations, the ASH:AWC activity ratio is higher (Fig. 4C), consistent with the idea that a lack of entrainment may reflect interference between AWC and ASH signals impinging on AVA.

To further support the idea that conflicting sensory signals may mask one another at the level of AVA, we measured EIs in TAX-4 animals. At the lowest [1-oct], the strong negative entrainment previously observed was abolished, confirming that negative entrainment is a function of TAX-4 signaling (Fig. 6E, F, H). At the intermediate [1-oct] (0.66 mM), *tax-4* loss of function mutation caused a slight positive shift in the EI, but did not lift it above the threshold for significant

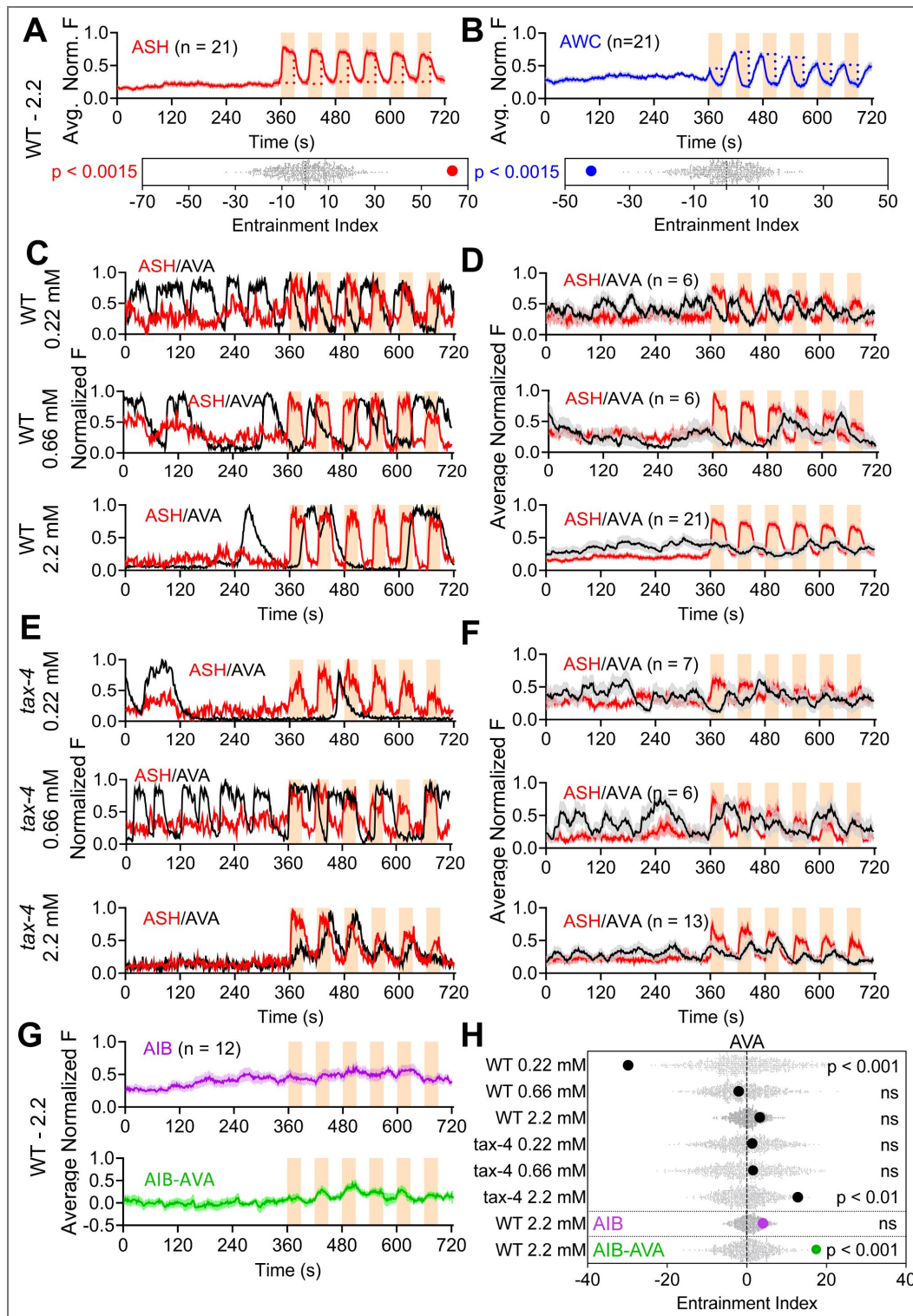


**Fig. 6. Entrainment of neuronal activity by 1-oct stimulation.**

(A, B) Validation of the entrainment index measurement using ASH (A) and AWC (B), showing very strong positive and very strong negative entrainment by 1-oct application, as expected. Gray dots indicate each randomized sum, while red and blue dots indicate the stimulus-specific sums of ASH and AWC, respectively (see Methods). (C-F) Superimposed ASH and AVA activity patterns after stimulation by 0.22, 0.66, and 2.2 mM 1-oct in wild type (C, D) and *tax-4* (E, F). Single worm traces (C, E) and averaged traces are shown (D, F, n ranges from 6-21 worms). (G) AIB traces (averaged); purple is unprocessed AIB signal, green is AIB minus AVA signal. (H) Entrainment indices for all recordings in C through G, with gray dots indicating randomized EIs and the bold dots represent the stimulus-specific EIs for AVA (black), unprocessed AIB (purple), and AVA-subtracted AIB (green). P values in A, B and H represent the probability that a randomized EI would be as great or greater than the stimulus-selected sum, with a significance cut-off of  $P < 0.05$ .

entrainment ( $P > 0.05$ ) (Fig. 6E, F, H [↗](#)). However, at the highest [1-oct], loss of TAX-4 positively shifted the EI into the significant range for positive entrainment (Fig. 6E, F, H [↗](#)). Interestingly, all of the calculated AVA EIs (Fig. 6H [↗](#)) correlate well with the overall chemotactic behavior in terms of sign (i.e. negative entrainment predicts attraction, positive entrainment predicts repulsion), even where the strength of entrainment with the sensory input did not exceed our set threshold for non-random entrainment (see Discussion). Most importantly, these results imply that the reverse command interneurons under these assay conditions will not necessarily show overt entrainment to sensory stimuli even though they are receiving sensory inputs because sensory stimuli may be encoded as parallel antagonistic afferent inputs which cancel one another out, until the prevailing conditions permit one input to become substantially stronger than the other.

To investigate how the 1-oct sensory signals are transmitted to AVA, we examined the interneuron AIB, which is positioned to be an integrating hub in this system because it receives afferent inputs from ASH, AWC, and many other sensory neurons, and from RIM, which provides feedback about the motor state that is used in the regulation of sensory afferent pathways by corollary discharge ([54](#), [75](#), [76](#)). Initially, we did not observe significant entrainment of AIB activity with 2.2 mM 1-oct application (Fig. 6G [↗](#)). It is possible that immobilization and anesthetization may be affecting AIB responses to sensory activity and/or proprioceptive feedback from locomotion. However, it is also possible that motor feedback from RIM was obscuring the sensory signal. To address this possibility, we subtracted AVA activity, representing the motor state, from the AIB activity (AVA closely mirrors RIM), based on the observation that AIB activity can be modeled as the sum of convolutions of motor activity and sensory activity ([77](#)). This modified AIB signal showed significant entrainment with 2.2 mM 1-oct application which was positive in sign (Fig. 6G [↗](#) and H [↗](#)), and greater than AVA's entrainment at the same 1-oct concentration. These observations suggest that AIB serves as a sensory relay for the aversive inputs, but since aversive entrainment in AVA is weaker than that in AIB (presumably due to interference from attractive inputs), the site of integration between repulsive and attractive pathways must be downstream of AIB and either at or upstream of AVA.

## Combinatorial olfactory coding facilitates context-dependent behavioral flexibility

What benefit might *C. elegans* gain from encoding 1-oct combinatorially, simultaneously activating attractive and repulsive afferent input pathways? This strategy could create a simple and versatile mechanism to modulate the behavioral output to best match internal and external conditions, such as specific odorant concentration, the presence of other odorants, or interoceptive inputs such as hunger or stress. A combinatorial strategy allows response sensitivity and even valence to be altered by simply adjusting gains or synaptic outputs within each pathway (Fig. 7A, B [↗](#)), without requiring extensive functional reorganization of the downstream connections, or recruitment of complex cross-inhibitory circuitry. For example, in the laboratory, 1-oct is used as a repellent for *C. elegans*, but its presence in the environment may convey more complex information. 1-oct is toxic to worms (thus representing a risk), which presumably explains why *C. elegans* has evolved to avoid it, at least at higher concentrations. However, 1-oct is naturally found in decaying plant material ([78](#), [79](#)), so it may also signal the presence of a bacterial food source for worms (thus representing a reward as well). In the presence of non-toxic alternatives, other food sources are safer, but in the absence of alternatives, worms may risk toxicity to avoid starvation. Could combinatorial coding support the risk-reward decision making required of *C. elegans* when evaluating environmental 1-oct signals? Consistent with this idea, many attractive food signals, including isoamyl alcohol (IAA), suppress AWC activity ([35](#), [39](#), [61](#)), and could therefore decrease the activity of the attractive afferent pathway to disinhibit repulsion (Fig. 7A, B [↗](#)). We tested this hypothesis by conducting chemotaxis experiments at 0.66 mM 1-oct, normally an attractive concentration in our microfluidics assays, in the presence of isoamyl alcohol (IAA,  $10^{-4}$  dilution, added to both the 1-oct and control buffer sides of the microfluidics arena). Under these conditions, worms were strongly repelled by 1-oct (Fig. 7C [↗](#)). The probability of reversals when entering the 1-oct zone was increased (Fig. 7D [↗](#)), the probability of reversals when exiting the 1-

oct zone was decreased (Fig. 7D [↗](#)), and the repulsion-inducing modulation of locomotory speed was also increased (Fig. 7E, F [↗](#)). Interestingly 0.66 mM 1-oct did not cause a speed increase on its own (unlike 2.2 mM, Fig. 5 [↗](#)). Acute application of IAA also did not affect speed. However, 0.66 mM 1-oct in the presence of IAA caused a large speed increase (2-fold). Since IAA reduces AWC activity, this IAA effect is consistent with removal of AWC inhibition of 0.66 mM 1-oct-dependent speed modulation. These three quantitative changes in locomotory parameters will each shift the chemotaxis index in the negative direction, converting 1-oct attraction to repulsion.

In network recordings, the presence of IAA greatly increased the sensory entrainment of AVA, positively correlating with stimulus application. This effect suggests that IAA will potentiate 1-oct avoidance by klinokinesis, or in other words, increasing the probability that worms will execute a reversal when they experience positive  $d[1\text{-oct}]/dt$ . These results provide proof-of-principle that rebalancing the afferent input pathways to reduce attraction and promote repulsion can control chemotaxis in an ethologically relevant manner and demonstrate the potential utility and flexibility of the combinatorial coding strategy.

## Discussion

We have investigated the response of *C. elegans* to the odorant 1-oct, using a combination of microfluidics-based behavioral analysis and whole-network  $\text{Ca}^{++}$  imaging.  $\text{Ca}^{++}$  imaging using the NeuroPAL system ([30](#)) showed that 1-oct activates at least 11 different sensory neurons including neurons associated with chemorepulsion and chemoattraction. 1-oct activates the ASH and AWC sensory neurons, with ON- and OFF-response kinetics, respectively. Paradoxically, this pattern suggests that sensory signals are being generated to simultaneously promote and inhibit locomotory reversals upon both 1-oct onset and offset. Based on this observation, we hypothesized that 1-oct may simultaneously activate repulsive and attractive afferent pathways, with the ultimate chemotactic outcome being determined by the balance between them. We tested this hypothesis using several approaches to selectively modulate the input pathways, such as varying 1-oct concentration, mutating key proteins in sensory signaling pathways, and selectively inactivating ASH and AWC chemogenetically. We observed that decreasing the repulsive drive unmasked attractive responses, and vice versa, indicating that balancing attractive and repulsive sensory afferent pathways control wild type 1-oct responses over at least a ten-fold concentration range. This novel insight highlights the value of the whole-brain approach (enabled by the NeuroPAL system) for studying the network dynamics underlying sensory driven behaviors.

Three distinct locomotory transitions appear to be important for the overall chemotactic outcome: reversals stimulated upon entering the 1-oct zone ('entry reversals'), reversals stimulated upon exiting the 1-oct zone ('exit reversals'), and increased locomotory activity within the 1-oct zone ('speed increase') (Fig. 8A [↗](#)). Based on numerical simulations, speed increase was the most important factor: reversal patterns at the highest 1-oct concentration clearly favored attraction but increased locomotory activity within the 1-oct zone overcame this bias and caused repulsion. Our results suggest that both repulsive and attractive afferent pathways may be involved in regulating these key locomotory transitions (Fig. 8A [↗](#)). Entry reversals were reduced in *osm-9* mutants but increased in *tax-4* mutants. Exit reversals were reduced in *tax-4* mutants (but not affected in *osm-9*). Speed increase was dependent on 1-oct concentration (akin to the activity of the repulsive input pathway) and potentiated under conditions in which depress the activity of AWC (a key sensory neuron in the attractive pathway).

Our chemogenetic data provide strong evidence that ASH and AWC contribute significantly to the repulsive and attractive input pathways, respectively. However, we cannot rule out the possible contributions of other sensory neurons. The promoters used for transgenic expression of HisCl1 are active in a few other neurons (i.e. *Psra-6* is active in ASI and *ceh-36* is active in ASE). However, these neurons showed little to no 1-oct responsiveness. For the repulsive pathway, the minimal effects due to loss of OSM-9 suggest that repulsive drive may also be provided by TAX-4-positive neurons (with the caveat that some ASH signaling remains in *osm-9* mutants) ([38](#), [67](#)). AWB and BAG are candidates based on their consistent 1-oct responses and the observation that AWB contributes to avoidance responses to volatile 1-oct ([34](#)). For the attractive pathway, chemogenetic

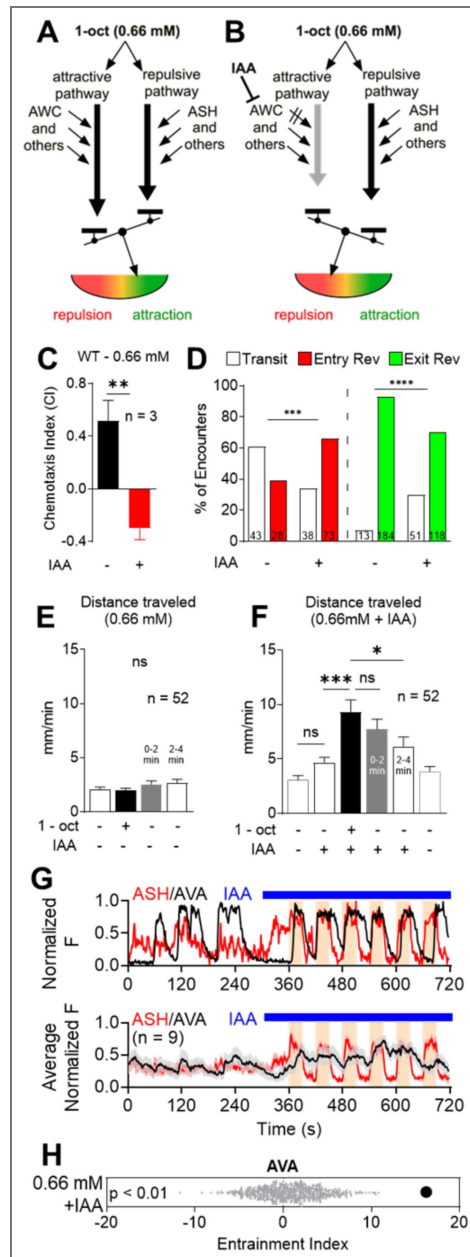


**Fig. 7. Balanced repulsion and attraction support context-dependent modulation of sensory responses.**

(A, B) Combinatorial coding-based mechanism for modulating sensory responses. (A) At lower 1-oct concentrations, the attractive afferent pathway is relatively strong, resulting in attraction. (B) Addition of IAA reduces AWC activity, weakening the attractive pathway relative to the repulsive pathway, and reversing the 1-oct valence. (C) Addition of 0.92 mM IAA reverses the valence of 1-oct (0.66 mM) from attractive to repulsive. (D) IAA biases reversal behavior (at the 1-oct/buffer interface) toward repulsion. Reversals upon entering 1-oct zone are increased (left side/red), and reversals upon exiting the 1-oct zone are decreased (right side/green). (E-F) Effect of IAA on locomotory activity. (E) 1-oct (0.66 mM) in the absence of IAA does not cause increased speed. (F) 1-oct (0.66 mM) in the presence of IAA causes markedly increased speed. (G) Single (upper) and averaged (lower) recordings of ASH and AVA before and after addition of IAA and 1-oct (0.66mM) as shown, demonstrating increased AVA entrainment to stimulus (compare to Fig-6D /middle). Blue bar indicates addition of IAA (in both control buffer and 1-oct solutions). (H) AVA entrainment index confirms that the presence of IAA causes AVA to become significantly entrained with the stimulus. \*\* in C indicates  $P < 0.01$ , *t*-test; \*\*\* and \*\*\*\* in D indicate  $P < 0.001$ ,  $0.0001$  respectively, Fisher's Exact Test; \*, \*\*\* in F indicate  $P < 0.05$  and  $0.001$ , respectively, ANOVA and Tukey's multiple comparison test.

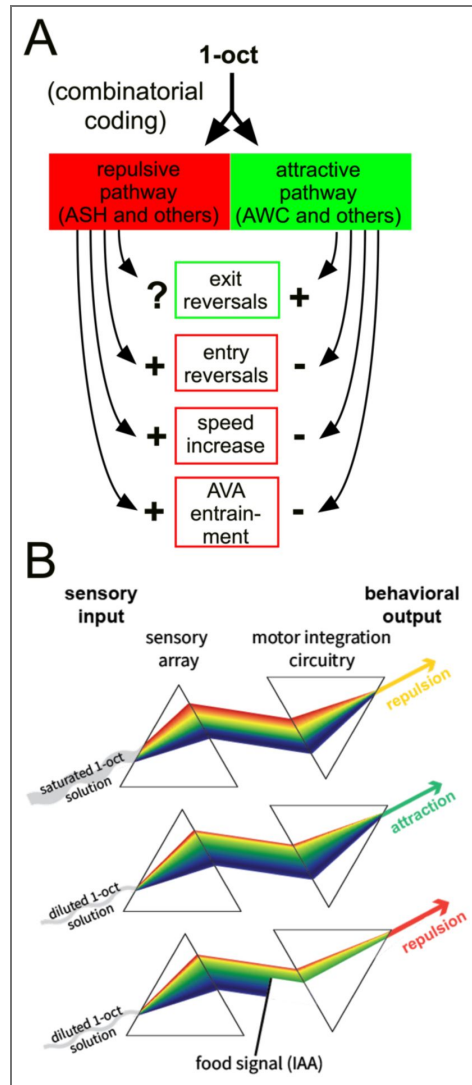


**Fig 8. Combinatorial coding of 1-oct as an attractant and a repellent, simultaneously, facilitates sensory motor coupling and context-dependent modulation in *C. elegans*.**

(A) 1-oct simultaneously activates sensory neurons in the periphery that mediate both repulsion (ASH and others) and attraction (AWC and others), such that repulsive and attractive afferent pathways become active concurrently. These inputs are then integrated centrally to control at least three key locomotory parameters (exit reversals, entry reversals, and locomotory speed), and the activity state of the reverse command neurons. (B) An analogy based on refraction on light through two prisms highlights the potential versatility of olfactory combinatorial coding in *C. elegans*. An individual odorant activates many chemosensory neurons to produce multiple distinct afferent inputs propagating through the downstream circuitry simultaneously, analogous to the first prism separating white light into its component colors (top panel, left). The motor integration circuitry formulates a locomotory response by integrating the active afferent pathways, analogous to the second prism recombining the incoming light (top panel, right). Because chemosensory neurons have different odorant affinities, the specific outputs of the sensory array and motor integration circuit may be concentration dependent. In this study, ASH (coded in red) is a low affinity sensor, while AWC (coded in blue) is a high affinity sensor. Reducing the 1-oct concentration biases the output of the sensory array toward AWC (middle panel, left), and the motor integration circuitry uses this information to produce an attractive locomotory response (middle panel, right). This coding strategy produces a simple framework for modulation. The behavioral outcome may be influenced by simply shifting the balance of the afferent pathways, much like an optical filter placed in a light path can selectively eliminate specific wavelengths (lower panel) to change the color of the transmitted light. In this study, IAA was added to the diluted 1-oct solution, inhibiting AWC, such that the afferent pathways were re-balanced toward the ASH end of the spectrum, and repulsion was restored. This ‘filtering’ effect could, in principle, take place peripherally or centrally, and could subserve modulation due to the presence of other odorant molecules, monoamine/neuropeptide modulators serving as interoceptive signals, and effectors of experience-dependent plasticity.

inactivation of AWC produced a modest effect relative to loss of TAX-4, implying there may be other TAX-4-dependent neurons contributing. We also cannot rule out a role for AWA, an OSM-9-dependent neuron associated with chemoattraction to soluble compounds. More generally, any sensory neuron which consistently responds to 1-oct addition or withdrawal has the potential to contribute to the behavioral response. Systematic mapping of sensory neuron contributions, individually and in combination, to the locomotory transitions and sensory-driven activity patterns in the downstream neural circuitry will be important to fully understand how *C. elegans* generates its behavioral response to 1-oct, and eventually other odorant classes.

Our results show how combinatorial and labeled line coding schemes may functionally interact. 1-oct is encoded combinatorially, in that it activates multiple sensory neurons (our results, and (39)), principally ASH and AWC. However, these neurons have long been regarded to represent repulsive and attractive labeled lines, respectively (33, 35, 38, 80). Thus, the initial combinatorial representation of 1-oct superimposes on the underlying labeled line architecture to dictate the final chemotactic outcome. The novel finding here is that multiple labeled lines become activated simultaneously in the context of a combinatorially-coded odorant. Previous studies have shown that antagonistic sensory inputs can contribute to chemosensory responses in *C. elegans* (81–84), but this study is the first to show in detail how conflicting inputs interact at the behavioral and circuit levels. The labeled lines independently control multiple locomotory parameters, in opposite directions, and the conflict is resolved by the locomotory system which is sensitive to the balance of the two pathways.

The compact size of the *C. elegans* nervous system makes it feasible to characterize at a cellular and molecular level where and how these afferent pathways converge and interact. Both pathways ultimately impinge on the AVA locomotory command interneurons, which drive locomotory reversals (85, 86). Because AVA sensory entrainment varies smoothly as a function of the relative activity levels of the two pathways, they probably do not strongly cross-inhibit one another, which would likely produce much steeper transitions (87). Which neurons are likely to integrate the attractive and repulsive inputs? Based on the connectome and previous functional studies, the AIB interneuron is a logical candidate. AIB is a first layer interneuron that receives extensive inputs from sensory neurons including ASH and AWC, strong synaptic inputs from other first layer interneurons (AIZ, AIA), and electrical and chemical synapses from locomotory command neurons AVE and RIM. AIB sends projections to the locomotory command neurons including AVA, RIM, and AVB (63, 88). Functionally, AIB serves as an integrating hub for multiple sensory inputs including ASH and AWC (89, 90). However, AIB does not appear to play the role of an integrating hub upstream of AVA for 1-oct. Prior to sensory stimulation, AIB activity closely followed reverse command interneuron activity, as has been observed previously (23, 54). Upon stimulation, AIB still followed the reverse command interneurons, but subtracting the reverse command signal from the AIB excitation pattern revealed that AIB was significantly entrained to the repulsive sensory input. AVA did not show this repulsive entrainment under the same conditions, therefore AIB cannot be the sole locus for integration. One intriguing possibility is that integration takes place in AVA itself, since it receives strong synaptic inputs directly from ASH, and from SAA, which mirrors the activity pattern of AWC during stimulation.

This coding scheme facilitates olfactory plasticity because the balance of the pathways, evaluated centrally, can determine odor valence. This plasticity differs from what has previously been described, where odorant responses are modulated at the periphery through lateral interactions among sensory afferents (20, 35) or reprogramming of individual sensory neuron responses (47). The broad versatility of this coding scheme can be appreciated by considering combinatorial coding and integration of inputs as analogous to the refraction of light through two prisms (Fig. 8B [↗](#)). First, the chemosensory neuron array in *C. elegans* creates a multi-factorial representation of the sensory stimulus, (i.e. the first prism), differentiating inputs from multiple sensory neurons, each with different downstream behavioral correlates. Downstream, the different components of this representation will eventually converge and become integrated into a coherent behavioral response by the motor command circuitry (i.e. the second prism). Because the sensory neurons have different concentration-response profiles, worms can easily generate differential behaviors

dependent on stimulus concentration: as concentration is reduced, the input from the sensory layer will be skewed toward the higher-affinity components (Fig. 8B [↗](#)). In this study, reduced [1-oct] favored the AWC-driven response (higher affinity) over the ASH-driven response (lower affinity), converting the 1-oct response from repulsion to attraction. This architecture also provides straightforward avenues for modulation. Multiple sensory inputs may be integrated if the additional odorants modulate the initial sensory representation, either additively (via ON neurons) or subtractively (via OFF neurons Fig. 8B [↗](#)). Here, the addition of IAA restored repulsion at lower concentrations by reducing the contribution of AWC. In the two-prism analogy, IAA is equivalent to a selective optical filter placed in the light path, skewing the overall balance back toward ASH. Other forms of plasticity, such as monoamine and neuropeptide modulation or experience dependent plasticity, may also be easily incorporated into this scheme at the sensory- or interneuron level. In a complex natural environment, where multiple odorants, interoceptive inputs, and experience-dependent plasticity are all acting simultaneously on a limited set of neurons, potential interference among modulatory signals might be avoided by funneling all the modulatory influences through one major repulsive pathway and one major attractive pathway.

## Materials and Methods

Key Resources Table				
Reagent type (species) or resource	Designation	Source or reference	Identifiers	Additional information
Strain, strain background ( <i>Escherichia coli</i> )	OP50	Caenorhabditis Genetics Center (CGC)	OP50	
Strain, strain background ( <i>C. elegans</i> )	Wild type	Caenorhabditis Genetics Center (CGC)	N2	
Strain, strain background ( <i>C. elegans</i> )	otIs669 V, otIs672 [rab-3::NLS::GCaMP6s + arrd-4::NLS::GCaMP6s]	Caenorhabditis Genetics Center (CGC)	OH15500	(30)
Strain, strain background ( <i>C. elegans</i> )	otIs669 V, wtfIs145 [rab-3p::his-24::GCaMP6s::unc-54 3' UTR + pBX]	Caenorhabditis Genetics Center (CGC)	AML320	
Strain, strain background ( <i>C. elegans</i> )	tax-4 (ok3771) III	Caenorhabditis Genetics Center (CGC)	VC3113	
Strain, strain background ( <i>C. elegans</i> )	tax-4 (ok3771) III, otIs669 V, wtfIs145 [rab-3p::his-24::GCaMP6s::unc-54 3' UTR + pBX]	This study	FY1041	
Strain, strain background ( <i>C. elegans</i> )	njEx1547[ceh-36p::HisC11::SL2::GFP, ges-1p::NLS::TagRFP]	<i>Ikeda et al. (2020)</i>	IK3591	(68)

Strain, strain background ( <i>C. elegans</i> )	kyEx5104 [sra-6p::HisC11::SL2::mCherry), 50 ng/μL + elt-2::mCherry, 1 ng/μL]	<i>Pokala et al. (2014)</i>	CX15206	(69)
Chemical compound, drug	Sylgard 184	Electron Microscopy Sciences	Cat# 24236 – 10	
Chemical compound, drug	Tetramisole hydrochloride	Sigma	CAS# 16595-80-5)	
Software, algorithm	Adobe Premier Pro	Adobe Inc.	<a href="https://www.adobe.com/">https://www.adobe.com/</a>	
Software, algorithm	Multi-Worm Tracker	<i>Itskovits et. al. (2017)</i>	<a href="https://github.com/itskov/MultiAnimalTrackerSuite">https://github.com/itskov/MultiAnimalTrackerSuite</a>	(70)
Software, algorithm	Mathematica	Wolfram Research	<a href="https://www.wolfram.com/">https://www.wolfram.com/</a>	
Software, algorithm	MATLAB	MathWorks	<a href="https://www.mathworks.com">https://www.mathworks.com</a>	
Software, algorithm	R	Posit PBC	R-Studio v2022.07.1	

Software, algorithm	Fiji/ImageJ	<i>Schindelin et al. (2012)</i>	<a href="https://imagej.net/software/fiji/downloads">https://imagej.net/software/fiji/downloads</a>	(91)
Software, algorithm	Graphpad	GraphPad Software	Prism 10.2.3	
Software, algorithm	MoCo plugin	<i>Dubbs et al. (2016)</i>	<a href="https://github.com/NTC-Columbia/moco">https://github.com/NTC-Columbia/moco</a>	(92)
Software, algorithm	WormLab tracking software	MBF Biosciences	<a href="https://www.mbfioscience.com">https://www.mbfioscience.com</a>	
Other	Silicon microfluidics masters	S. Lockery and D. Albrecht		
Other	Olfactory chips	Microkosmos	<a href="http://ukosmos.com">ukosmos.com</a>	(53)

## Worm maintenance and strains

*C. elegans* were maintained at 20°C on NGM agar plates and fed *E. coli* OP50 bacteria. All experiments were conducted at 20-22°C (93, 94). The following strains were utilized:

**N2:** Wild-type.

**OH15500:** otIs669 V, otIs672 [rab-3::NLS::GCaMP6s + arrd-4::NLS::GCaMP6s] (30).

**AML320:** otIs669 V, wtfIs145 [rab-3p::his-24::GCaMP6s::unc-54 3' UTR + pBX].

**VC3113:** tax-4 (ok3771) III.

**CX10:** osm-9 (ky10) IV.

**FY1041:** tax-4 (ok3771) III, otIs669 V, wtfIs145 [rab-3p::his-24::GCaMP6s::unc-54 3' UTR + pBX].

**IK3591:** njEx1547[ceh-36p::HisCl1::SL2::GFP, ges-1p::NLS::TagRFP]

**CX15206:** kyEx5104[sra-6p::HisCl1::SL2::mCherry, 50 ng/μL + elt-2::mCherry, 1 ng/μL]

Strains were obtained from the Caenorhabditis Genetics Center (CGC), funded by NIH (P40 OD010440). VC3113 was crossed into AML320 to generate FY1041, with the presence of *tax-4* verified by PCR. Strains were allowed for three generations of growth before experiments.

## Microfluidics device fabrication and behavioral assays

All behavioral studies were conducted in microfluidic devices following standard protocols (49–51). Devices were fabricated by thoroughly mixing polydimethylsiloxane (PDMS) and a curing agent in a 10:1 ratio by weight (Sylgard 184, Electron Microscopy Sciences Cat. 24236 – 10), degassing the mixture under vacuum, and then pouring it onto a silicon mold at ~5 mm height. PDMS was cured by incubating at 65°C for at least 3 hours. Olfactory chips were obtained from Microkosmos ([ukosmos.com](https://www.ukosmos.com)).

### Chemotaxis

Chemotaxis assays utilized a ‘two-chamber’ device dividing the arena into equal chambers for stimulus and control buffer (S-basal [100mM NaCl, 5mM g K<sub>2</sub>HPO<sub>4</sub>, 45mM KH<sub>2</sub>PO<sub>4</sub>, pH = 6]) (49). Worm behavior was recorded using AmScope microscope cameras (MD 500, MU 500-HS, AmScope, Irvine, CA), and videos were processed using Adobe Premier Pro 2024 (Adobe Inc., San Jose, CA). 1-2 day old adults were picked and washed with S-basal and loaded into the microfluidics arena. Animals were acclimatized in the arena for 5 minutes; assays were performed between 20-40 minutes from starvation onset while they were in area-restricted search foraging mode (52). In the original microfluidics protocols (50, 51) 0.01% w/v xylene cyanol (0.1mg/ml) dye was used to verify clean separation between different domains within the microfluidics device. However, worms show clear attraction to 0.01% xylene cyanol (data not shown), indicating that the presence of dye introduces an additional olfactory stimulus. Therefore, we modified the protocol to test the flow pattern using dye before and after the assay but remove the dye during the assay (Fig 1A). In control trials using dye, we verified that flow patterns stay stable for up to 90 minutes once properly established. If the flow pattern in the post-data collection dye test was compromised, data were rejected. Histamine incubation was performed as previously described (69). Chemotaxis index was calculated between 10-20 minutes of stimulus onset, using the equation: Chemotaxis Index (CI) = (Number of worms in stimulus – Number of worms in buffer)/Total number of worms, positive and negative indices representing attraction and aversion respectively.

### Distance traveled

Locomotory distance-traveled assays used the ‘two-chamber’ device (49) with both chambers containing the same solution. Worms were exposed sequentially to buffer (5 mins), stimulus (5 mins), and buffer (10 mins). A complete exchange of solutions takes approximately 1 minute. Data were collected 90 seconds after solution change to ensure complete exchange. Distance traveled per minute was recorded over 2 minutes in buffer (pre-stimulus), in 1-oct solution (stimulus), and in successive 2-minute intervals after 1-oct withdrawal (post-stimulus). Worm tracks were manually traced and measured using Adobe Premiere Pro 2024 and Graphic for Mac (Autodesk, San Francisco, CA).

Worm locomotion simulation was written in Mathematica using AI-enabled chat (Mathematica, Princeton NJ). In the simulation, 20 one-dimensional dots, representing worms, were allowed to travel a one-dimensional line, representing behavior arena. The line was divided equally into two zones, representing buffer and stimulus, and dots moved freely within the line with random reversal frequency. Dot speed increased in the stimulus zone, as indicated, and reversal frequency at the interface was specified as observed from behavioral assays. 10 simulations were performed and averaged for each speed differential shown in Fig. 5F.

### Reversals

Analyses of locomotory reversals were performed using larger ‘stripe’ chips (50), which provided a greater working area and facilitated automated video tracking by reducing the frequency of collisions between worms. These chips were usually configured with 3 zones of equal size: a stripe of 1-oct down the middle flanked on either side by buffer, although for some experiments, the 1-oct was placed on one side. Video recordings of worm behavior were analyzed using the Multi-Worm Tracker (95) using MatLab (Mathworks, Natick, MA), or the WormLab tracker (MBS Biosciences, Williston VT), with manual analysis of individual tracks to quantify reversals.

## Whole-brain calcium imaging

Neuronal activity was examined by measuring calcium transients detected by fluorescence change (GCaMP6s, OH15500 (30), AML320 (96)). Calcium imaging was conducted as previously described (23, 53, 54). Animals were anesthetized with 1 mM tetramisole hydrochloride (Sigma, CAS 16595-80-5) in S-basal buffer and imaged in PDMS olfactory microfluidic devices, which trap the worm in a chemical delivery system and provides inlets to deliver either buffer or stimulus to the nose using laminar flow (53). Head-ganglia neurons were recorded using Leica confocal microscope (SP8) at 0.6 - 0.8 Hz rate. Odorants were diluted in S-basal. Each worm was recorded for 12-14 minutes within 20-40 minutes from starvation onset, starting with 6 minutes of buffer exposure followed by 6-7 30-second pulses of stimulus with 30-second intervals. Calcium imaging was followed by immediate recording of NeuroPAL color markers. For +IAA experiments, IAA delivery to the nose was started after 5 minutes of recording (1 minute before the first stimulus application) and IAA was present in the stimulus and buffer channels thereafter. For concentration-response of ASH and AWC experiments, three 0.22 mM, two 0.66 mM and two 2.2 mM 1-sec pulses were given serially to the same worm; repeated application produced identical response amplitudes.

Recorded image files were stacked and analyzed using Fiji/ImageJ (91) followed by motion correction with 'MoCo' plug-in (92). Neuron identity was manually assigned and matched with calcium response using guidelines described by Yemini and Hobert (30). Neurons with ambiguous identities were excluded from the analysis (Fig. 2). Individual neuron activity was then normalized and re-sampled, before averaging, by 'Min-Max normalization' and 'Linear interpolation' respectively, using custom R-scripts (97).

## Data analyses and statistics

Statistical analyses were performed using Prism v10.2.1 (GraphPad Software Inc., La Jolla, CA), R v4.3, R-Studio v2022.07.1 (Posit PBC, Boston, MA), MatLab vR2023A (MathWorks, CA) and Microsoft Excel 2016. Chemotaxis assays were repeated 3-5 times and analyzed by *Student's t-test* (unpaired). Pooled data from distance-traveled assays were analyzed by one-way ANOVA with post-tests. Reversal assays were repeated 3 times, data were pooled, and analyzed using Fisher exact tests.

Entrainment indices (EIs) were calculated using averaged, normalized calcium responses. First, area-under-curve (AUC) values were calculated for all possible 30s epochs by summing the  $Ca^{++}$  signal intensities over 30s after first subtracting the corresponding initial  $Ca^{++}$  signal intensity. EIs were calculated by adding six AUCs; stimulus-dependent EIs were calculated by adding the six AUCs corresponding to stimulus application intervals, while random EIs were calculated by adding six randomly-chosen AUCs. The significance of stimulus entrainment was estimated as the probability that the stimulus-dependent EI would exceed any given random EI, with probabilities < 0.05 considered significant (i.e.  $P < 0.05$ ). A P value < 0.0015 indicated that the experimental EI was larger (or smaller) than all possible random EIs within the dataset. EIs for AVA were calculated using a 10-second lag, across all conditions, because, where obvious sensory entrainment was seen, AVA signals showed consistently slowed responses compared to sensory signals. No lag was incorporated for sensory and first-layer interneurons (ASH, AWC, AIB).

Neuronal activity correlations were calculated using Spearman's rank correlation test and corrected with Fisher's z-transformation before testing statistical significance (98–100), using custom R scripts.

## Data availability

Dataset and code are available for download at [Zenodo.org](https://zenodo.org) (<https://doi.org/10.5281/zenodo.13328278>).

## Acknowledgements

We would like to thank Shawn Lockery and Dirk Albrecht for invaluable help and materials for the microfluidics behavioral assays, the *C. elegans* Genetics Center for strains (funded by NIH P40 OD010440), Ikue Mori for IK3591, Cori Bargmann for CX15206, Tomer Avidor-Reiss and Qian Chen for assistance with confocal microscopy,

## Additional information

### Funding

This work was funded by NIH grant 1R15DC022738-01 to BAB, and the University of Toledo Office of Research through the DeArce-Koch Memorial Foundation Award, the Small Award Program, and the Interdisciplinary Research Initiation Award. WGR was supported by NIH NIGMS T32-GRISE grant number 1T32GM144873-01. The funding sources were not involved in study design, data collection and interpretation, or the decision to submit the work for publication.

### Author contributions

Conceptualization: MZHS, BAB, WGR, RM. Software: BAB. Methodology: MZHS, BAB, CAE, LGJ. Investigation: MZHS, WGR, CAE, BNS, LA, JK, AM, ARM, RM, BAB. Data visualization: MZHS, WGR, BAB. Supervision: BAB, RM. Writing (original draft): MZHS, BAB. Funding acquisition BAB, RM, WGR.

### Funding

Funder	Grant reference number	Author
NIH/NIDCD	1R15DC022738-01	Bruce A Bamber
The University of Toledo Office of Research	Small Award Program	Bruce A Bamber
The University of Toledo Office of Research	DeArce Koch Memorial Foundation	Bruce A Bamber
The University of Toledo Office of Research	Interdisciplinary Research Initiation Award	Bruce A Bamber
NIH/NIGMS	1T32GM144873-01	William G Ryan

## References

1. Andersson M. N., Löfstedt C., Newcomb R. D. (2015) Insect olfaction and the evolution of receptor tuning. *Frontiers in Ecology and Evolution* **3**:53 <https://doi.org/10.3389/fevo.2015.00053>
2. Haverkamp A., Hansson B. S., Knaden M. (2018) Combinatorial codes and labeled lines: how insects use olfactory cues to find and judge food, mates, and oviposition sites in complex environments. *Frontiers in Physiology* **9**:49 <https://doi.org/10.3389/fphys.2018.00049> | [PubMed](#)
3. Grabe V., Sachse S. (2018) Fundamental principles of the olfactory code. *Biosystems* **164**:94-101 <https://doi.org/10.1016/j.biosystems.2017.10.010> | [PubMed](#)
4. Mori K., Sakano H. (2021) Olfactory circuitry and behavioral decisions. *Annual Review of Physiology* **83**:231-256 <https://doi.org/10.1146/annurev-physiol-031820-092824> | [PubMed](#)
5. Malnic B., Hirono J., Sato T., Buck L. B. (1999) Combinatorial receptor codes for odors. *Cell* **96**:713-723 [https://doi.org/10.1016/s0092-8674\(00\)80581-4](https://doi.org/10.1016/s0092-8674(00)80581-4) | [PubMed](#)
6. Touhara K., Vosshall L. B. (2009) Sensing odorants and pheromones with chemosensory receptors. *Annual review of physiology* **71**:307-332 <https://doi.org/10.1146/annurev.physiol.010908.163209> | [PubMed](#)
7. Wyatt T. D. (2014) Introduction to chemical signaling in vertebrates and invertebrates. In: Mucignat-Caretta C (Ed). *Neurobiology of Chemical Communication*

8. **Stensmyr M. C.**, Dweck H. K., Farhan A., Ibba I., Strutz A., Mukunda L., Linz J., Grabe V., Steck K., Lavista-Llanos S. (2012) A conserved dedicated olfactory circuit for detecting harmful microbes in *Drosophila*. *Cell* **151**:1345-1357 <https://doi.org/10.1016/j.cell.2012.09.046> | PubMed
9. **Ebrahim S. A.**, Dweck H. K., Stökl J., Hofferberth J. E., Trona F., Weniger K., Rybak J., Seki Y., Stensmyr M. C., Sachse S. (2015) *Drosophila* avoids parasitoids by sensing their semiochemicals via a dedicated olfactory circuit. *PLoS biology* **13**:e1002318 <https://doi.org/10.1371/journal.pbio.1002318> | PubMed
10. **Jiang H.-C.**, Park S. J., Wang I.-H., Bear D. M., Nowlan A., Greer P. L. (2024) CD20/MS4A1 is a mammalian olfactory receptor expressed in a subset of olfactory sensory neurons that mediates innate avoidance of predators. *Nature Communications* **15**:3360 <https://doi.org/10.1038/s41467-024-47698-3> | PubMed
11. **Saito H.**, Nishizumi H., Suzuki S., Matsumoto H., Ieki N., Abe T., Kiyonari H., Morita M., Yokota H., Hirayama N. (2017) Immobility responses are induced by photoactivation of single glomerular species responsive to fox odour TMT. *Nature communications* **8**:16011 <https://doi.org/10.1038/ncomms16011> | PubMed
12. **Horio N.**, Murata K., Yoshikawa K., Yoshihara Y., Touhara K. (2019) Contribution of individual olfactory receptors to odor-induced attractive or aversive behavior in mice. *Nature communications* **10**:209 <https://doi.org/10.1038/s41467-018-07940-1> | PubMed
13. **Cande J.**, Prud'homme B., Gompel N. (2013) Smells like evolution: the role of chemoreceptor evolution in behavioral change. *Current opinion in neurobiology* **23**:152-158 <https://doi.org/10.1016/j.conb.2012.07.008> | PubMed
14. **Buck L.**, Axel R. (1991) A novel multigene family may encode odorant receptors: a molecular basis for odor recognition. *Cell* **65**:175-187 [https://doi.org/10.1016/0092-8674\(91\)90418-x](https://doi.org/10.1016/0092-8674(91)90418-x) | PubMed
15. **Mombaerts P.**, Wang F., Dulac C., Chao S. K., Nemes A., Mendelsohn M., Edmondson J., Axel R. (1996) Visualizing an olfactory sensory map. *Cell* **87**:675-686 [https://doi.org/10.1016/s0092-8674\(00\)81387-2](https://doi.org/10.1016/s0092-8674(00)81387-2) | PubMed
16. **Blazing R. M.**, Franks K. M. (2020) Odor coding in piriform cortex: mechanistic insights into distributed coding. *Curr Opin Neurobiol* **64**:96-102 <https://doi.org/10.1016/j.conb.2020.03.001> | PubMed
17. **Pérez-Gómez A.**, Bleyemehl K., Stein B., Pyrski M., Birnbaumer L., Munger S. D., Leinders-Zufall T., Zufall F., Chamero P. (2015) Innate predator odor aversion driven by parallel olfactory subsystems that converge in the ventromedial hypothalamus. *Current Biology* **25**:1340-1346 <https://doi.org/10.1016/j.cub.2015.03.026> | PubMed
18. **Poo C.**, Agarwal G., Bonacchi N., Mainen Z. F. (2022) Spatial maps in piriform cortex during olfactory navigation. *Nature* **601**:595-599 <https://doi.org/10.1038/s41586-021-04242-3> | PubMed
19. **Chen Y.**, Chen X., Baserdem B., Zhan H., Li Y., Davis M. B., Kebschull J. M., Zador A. M., Koulakov A. A., Albeanu D. F. (2022) High-throughput sequencing of single neuron projections reveals spatial organization in the olfactory cortex. *Cell* **185**:4117-4134.e4128 <https://doi.org/10.1016/j.cell.2022.09.038> | PubMed
20. **Zocchi D.**, Emily S. Y., Hauser V., O'Connell T. F., Hong E. J. (2022) Parallel encoding of CO<sub>2</sub> in attractive and aversive glomeruli by selective lateral signaling between olfactory afferents. *Current Biology* **32**:4225-4239.e4227 <https://doi.org/10.1016/j.cub.2022.08.025> | PubMed
21. **Schrödel T.**, Prevedel R., Aumayr K., Zimmer M., Vaziri A. (2013) Brain-wide 3D imaging of neuronal activity in *Caenorhabditis elegans* with sculpted light. *Nature methods* **10**:1013-1020 <https://doi.org/10.1038/nmeth.2637> | PubMed
22. **Prevedel R.**, Yoon Y.-G., Hoffmann M., Pak N., Wetzstein G., Kato S., Schrödel T., Raskar R., Zimmer M., Boyden E. S. (2014) Simultaneous whole-animal 3D imaging of neuronal activity using light-field microscopy. *Nature methods* **11**:727-730 <https://doi.org/10.1038/nmeth.2964> | PubMed
23. **Kato S.**, Kaplan H. S., Schrödel T., Skora S., Lindsay T. H., Yemini E., Lockery S., Zimmer M. (2015) Global brain dynamics embed the motor command sequence of *Caenorhabditis elegans*. *Cell* **163**:656-669 <https://doi.org/10.1016/j.cell.2015.09.034> | PubMed

24. **Nguyen J. P.**, Shipley F. B., Linder A. N., Plummer G. S., Liu M., Setru S. U., Shaevitz J. W., Leifer A. M. (2016) Whole-brain calcium imaging with cellular resolution in freely behaving *Caenorhabditis elegans*. *Proceedings of the National Academy of Sciences* **113**:E1074-E1081 <https://doi.org/10.1073/pnas.1507110112> | PubMed
25. **Kotera I.**, Tran N. A., Fu D., Kim J. H., Byrne Rodgers J., Ryu W. S. (2016) Pan-neuronal screening in *Caenorhabditis elegans* reveals asymmetric dynamics of AWC neurons is critical for thermal avoidance behavior. *eLife* **5**:e19021 <https://doi.org/10.7554/eLife.19021> | PubMed
26. **Venkatachalam V.**, Ji N., Wang X., Clark C., Mitchell J. K., Klein M., Tabone C. J., Florman J., Ji H., Greenwood J. (2016) Pan-neuronal imaging in roaming *Caenorhabditis elegans*. *Proceedings of the National Academy of Sciences* **113**:E1082-E1088 <https://doi.org/10.1073/pnas.1507109113> | PubMed
27. **Nichols A. L.**, Eichler T., Latham R., Zimmer M. (2017) A global brain state underlies *C. elegans* sleep behavior. *Science* **356**:eaam6851 <https://doi.org/10.1126/science.aam6851> | PubMed
28. **Toyoshima Y.**, Wu S., Kanamori M., Sato H., Jang M. S., Oe S., Murakami Y., Teramoto T., Park C., Iwasaki Y. (2020) Neuron ID dataset facilitates neuronal annotation for whole-brain activity imaging of *C. elegans*. *BMC biology* **18**:1-20 <https://doi.org/10.1186/s12915-020-0745-2> | PubMed
29. **Hallinen K. M.**, Dempsey R., Scholz M., Yu X., Linder A., Randi F., Sharma A. K., Shaevitz J. W., Leifer A. M. (2021) Decoding locomotion from population neural activity in moving *C. elegans*. *eLife* **10**:e66135 <https://doi.org/10.7554/eLife.66135> | PubMed
30. **Yemini E.**, Lin A., Nejatbakhsh A., Varol E., Sun R., Mena G. E., Samuel A. D. T., Paninski L., Venkatachalam V., Hobert O. (2021) NeuroPAL: A Multicolor Atlas for Whole-Brain Neuronal Identification in *C. elegans*. *Cell* **184**:272-288.e211 <https://doi.org/10.1016/j.cell.2020.12.012> | PubMed
31. **Dag U.**, Nwabudike I., Kang D., Gomes M. A., Kim J., Atanas A. A., Bueno E., Estrem C., Pugliese S., Wang Z. (2023) Dissecting the functional organization of the *C. elegans* serotonergic system at whole-brain scale. *Cell* **186**:2574-2592.e2520 <https://doi.org/10.1016/j.cell.2023.04.023> | PubMed
32. **Bargmann C. I.**, Hartweg E., Horvitz H. R. (1993) Odorant-selective genes and neurons mediate olfaction in *C. elegans*. *Cell* **74**:515-527 [https://doi.org/10.1016/0092-8674\(93\)80053-h](https://doi.org/10.1016/0092-8674(93)80053-h) | PubMed
33. **Troemel E. R.**, Kimmel B. E., Bargmann C. I. (1997) Reprogramming chemotaxis responses: sensory neurons define olfactory preferences in *C. elegans*. *Cell* **91**:161-169 [https://doi.org/10.1016/s0092-8674\(00\)80399-2](https://doi.org/10.1016/s0092-8674(00)80399-2) | PubMed
34. **Chao M. Y.**, Komatsu H., Fukuto H. S., Dionne H. M., Hart A. C. (2004) Feeding status and serotonin rapidly and reversibly modulate a *Caenorhabditis elegans* chemosensory circuit. *Proc Natl Acad Sci U S A* **101**:15512-15517 <https://doi.org/10.1073/pnas.0403369101> | PubMed
35. **Yoshida K.**, Hirotsu T., Tagawa T., Oda S., Wakabayashi T., Iino Y., Ishihara T. (2012) Odour concentration-dependent olfactory preference change in *C. elegans*. *Nature communications* **3**:739 <https://doi.org/10.1038/ncomms1750> | PubMed
36. **Greene J. S.**, Dobosiewicz M., Butcher R. A., McGrath P. T., Bargmann C. I. (2016) Regulatory changes in two chemoreceptor genes contribute to a *Caenorhabditis elegans* QTL for foraging behavior. *eLife* **5**:e21454 <https://doi.org/10.7554/eLife.21454> | PubMed
37. **Rengarajan S.**, Hallem E. A. (2016) Olfactory circuits and behaviors of nematodes. *Current Opinion in Neurobiology* **41**:136-148 <https://doi.org/10.1016/j.conb.2016.09.002> | PubMed
38. **Ferkey D. M.**, Sengupta P., L'Etoile N. D. (2021) Chemosensory signal transduction in *Caenorhabditis elegans*. *Genetics* **217** <https://doi.org/10.1093/genetics/iyab004> | PubMed
39. **Lin A.**, Qin S., Casademunt H., Wu M., Hung W., Cain G., Tan N. Z., Valenzuela R., Lesanpezeshki L., Venkatachalam V., *et al.* (2023) Functional imaging and quantification of multineuronal olfactory responses in *C. elegans*. *Science Advances* **9**:eade1249 <https://doi.org/10.1126/sciadv.ade1249> | PubMed
40. **Ache B. W.**, Young J. M. (2005) Olfaction: diverse species, conserved principles. *Neuron* **48**:417-430 <https://doi.org/10.1016/j.neuron.2005.10.022> | PubMed

41. Troemel E. R., Chou J. H., Dwyer N. D., Colbert H. A., Bargmann C. I. (1995) Divergent seven transmembrane receptors are candidate chemosensory receptors in *C. elegans*. *Cell* **83**:207-218 [https://doi.org/10.1016/0092-8674\(95\)90162-0](https://doi.org/10.1016/0092-8674(95)90162-0) | PubMed
42. Wragg R. T., Hapiak V., Miller S. B., Harris G. P., Gray J., Komuniecki P. R., Komuniecki R. W. (2007) Tyramine and octopamine independently inhibit serotonin-stimulated aversive behaviors in *Caenorhabditis elegans* through two novel amine receptors. *Journal of Neuroscience* **27**:13402-13412 <https://doi.org/10.1523/jneurosci.3495-07.2007> | PubMed
43. Hapiak V., Summers P., Ortega A., Law W. J., Stein A., Komuniecki R. (2013) Neuropeptides amplify and focus the monoaminergic inhibition of nociception in *Caenorhabditis elegans*. *Journal of Neuroscience* **33**:14107-14116 <https://doi.org/10.1523/jneurosci.1324-13.2013> | PubMed
44. Zahratka J. A., Williams P. D., Summers P. J., Komuniecki R. W., Bamber B. A. (2015) Serotonin differentially modulates Ca<sup>2+</sup> transients and depolarization in a *C. elegans* nociceptor. *J Neurophysiol* **113**:1041-1050 <https://doi.org/10.1152/jn.00665.2014> | PubMed
45. Williams P. D., Zahratka J. A., Rodenbeck M., Wanamaker J., Linzie H., Bamber B. A. (2018) Serotonin disinhibits a *Caenorhabditis elegans* sensory neuron by suppressing Ca<sup>2+</sup>-dependent negative feedback. *Journal of Neuroscience* **38**:2069-2080 <https://doi.org/10.1523/jneurosci.1908-17.2018> | PubMed
46. Debnath A., Williams P. D., Bamber B. A. (2022) Reduced Ca<sup>2+</sup> transient amplitudes may signify increased or decreased depolarization depending on the neuromodulatory signaling pathway. *Frontiers in Neuroscience* **16**:931328 <https://doi.org/10.3389/fnins.2022.931328> | PubMed
47. Khan M., Hartmann A. H., O'Donnell M. P., Piccione M., Pandey A., Chao P.-H., Dwyer N. D., Bargmann C. I., Sengupta P. (2022) Context-dependent reversal of odorant preference is driven by inversion of the response in a single sensory neuron type. *PLoS biology* **20**:e3001677 <https://doi.org/10.1371/journal.pbio.3001677> | PubMed
48. Fryer E., Guha S., Rogel-Hernandez L. E., Logan-Garbisch T., Farah H., Rezaei E., Mollhoff I. N., Nekimken A. L., Xu A., Selin Seyahi L., et al. (2024) An efficient behavioral screening platform classifies natural products and other chemical cues according to their chemosensory valence in *C. elegans*. *bioRxiv* <https://doi.org/10.1101/2023.06.02.542933> | PubMed
49. Lockery S. R., Lawton K. J., Doll J. C., Faumont S., Coulthard S. M., Thiele T. R., Chronis N., McCormick K. E., Goodman M. B., Pruitt B. L. (2008) Artificial dirt: microfluidic substrates for nematode neurobiology and behavior. *Journal of neurophysiology* **99**:3136-3143 <https://doi.org/10.1152/jn.91327.2007> | PubMed
50. Albrecht D. R., Bargmann C. I. (2011) High-content behavioral analysis of *Caenorhabditis elegans* in precise spatiotemporal chemical environments. *Nat Methods* **8**:599-605 <https://doi.org/10.1038/nmeth.1630> | PubMed
51. Lagoy R. C., Albrecht D. R. (2015) Microfluidic devices for behavioral analysis, microscopy, and neuronal imaging in *Caenorhabditis elegans*. *C. elegans: Methods and Applications* 159-179 [https://doi.org/10.1007/978-1-4939-2842-2\\_12](https://doi.org/10.1007/978-1-4939-2842-2_12) | PubMed
52. Gray J. M., Hill J. J., Bargmann C. I. (2005) A circuit for navigation in *Caenorhabditis elegans*. *Proc Natl Acad Sci U S A* **102**:3184-3191 <https://doi.org/10.1073/pnas.0409009101> | PubMed
53. Chronis N., Zimmer M., Bargmann C. I. (2007) Microfluidics for in vivo imaging of neuronal and behavioral activity in *Caenorhabditis elegans*. *Nat Methods* **4**:727-731 <https://doi.org/10.1038/nmeth1075> | PubMed
54. Gordus A., Pokala N., Levy S., Flavell S. W., Bargmann C. I. (2015) Feedback from network states generates variability in a probabilistic olfactory circuit. *Cell* **161**:215-227 <https://doi.org/10.1016/j.cell.2015.02.018> | PubMed
55. Katz M., Corson F., Keil W., Singhal A., Bae A., Lu Y., Liang Y., Shaham S. (2019) Glutamate spillover in *C. elegans* triggers repetitive behavior through presynaptic activation of MGL-2/mGluR5. *Nature Communications* **10**:1882 <https://doi.org/10.1038/s41467-019-09581-4> | PubMed

56. Wirak G. S., Florman J., Alkema M. J., Connor C. W., Gabel C. V. (2022) Age-associated changes to neuronal dynamics involve a disruption of excitatory/inhibitory balance in *C. elegans*. *eLife* **11**:e72135 <https://doi.org/10.7554/eLife.72135> | PubMed
57. Sordillo A., Bargmann C. I. (2021) Behavioral control by depolarized and hyperpolarized states of an integrating neuron. *eLife* **10**:e67723 <https://doi.org/10.7554/eLife.67723> | PubMed
58. Li Z., Zhou J., Wani K. A., Yu T., Ronan E. A., Piggott B. J., Liu J., Xu X. S. (2023) A *C. elegans* neuron both promotes and suppresses motor behavior to fine tune motor output. *Frontiers in Molecular Neuroscience* **16** <https://doi.org/10.3389/fnmol.2023.1228980> | PubMed
59. Meng J., Ahamed T., Yu B., Hung W., Mouridi S. El, Wang Z., Zhang Y., Wen Q., Boulin T., Gao S. (2024) A tonically active master neuron modulates mutually exclusive motor states at two timescales. *Science Advances* **10**:eadk0002 <https://doi.org/10.1126/sciadv.adk0002> | PubMed
60. Kato S., Kaplan H. S., Schrodell T., Skora S., Lindsay T. H., Yemini E., Lockery S., Zimmer M. (2015) Global brain dynamics embed the motor command sequence of *Caenorhabditis elegans*. *Cell* **163**:656-669 <https://doi.org/10.1016/j.cell.2015.09.034> | PubMed
61. Chalasani S. H., Chronis N., Tsunozaki M., Gray J. M., Ramot D., Goodman M. B., Bargmann C. I. (2007) Dissecting a circuit for olfactory behaviour in *Caenorhabditis elegans*. *Nature* **450**:63-70 <https://doi.org/10.1038/nature06292> | PubMed
62. Im Choi J., Lee H. K., Kim H. S., Park S. Y., Lee T. Y., Yoon K.-h., Lee J. I. (2018) Odor-dependent temporal dynamics in *Caenorhabditis elegans* adaptation and aversive learning behavior. *PeerJ* **6**:e4956 <https://doi.org/10.7717/peerj.4956> | PubMed
63. White J. G., Southgate E., Thomson J. N., Brenner S. (1986) The structure of the nervous system of the nematode *Caenorhabditis elegans*. *Philos Trans R Soc Lond B Biol Sci* **314**:1-340 <https://doi.org/10.1098/rstb.1986.0056> | PubMed
64. White J. (2018) Clues to basis of exploratory behaviour of the *C. elegans* snout from head somatotropy. *Philos Trans R Soc Lond B Biol Sci* **373** <https://doi.org/10.1098/rstb.2017.0367> | PubMed
65. Ouellette M.-H., Desrochers M. J., Gheta I., Ramos R., Hendricks M. (2018) A gate-and-switch model for head orientation behaviors in *Caenorhabditis elegans*. *Eneuro* **5** <https://doi.org/10.1523/eneuro.0121-18.2018> | PubMed
66. Colbert H. A., Smith T. L., Bargmann C. I. (1997) OSM-9, a novel protein with structural similarity to channels, is required for olfaction, mechanosensation, and olfactory adaptation in *Caenorhabditis elegans*. *J Neurosci* **17**:8259-8269 <https://doi.org/10.1523/jneurosci.17-21-08259.1997> | PubMed
67. Ezak M. J., Hong E., Chaparro-Garcia A., Ferkey D. M. (2010) *Caenorhabditis elegans* TRPV channels function in a modality-specific pathway to regulate response to aberrant sensory signaling. *Genetics* **185**:233-244 <https://doi.org/10.1534/genetics.110.115188> | PubMed
68. Ikeda M., Nakano S., Giles A. C., Xu L., Costa W. S., Gottschalk A., Mori I. (2020) Context-dependent operation of neural circuits underlies a navigation behavior in *Caenorhabditis elegans*. *Proc Natl Acad Sci U S A* **117**:6178-6188 <https://doi.org/10.1073/pnas.1918528117> | PubMed
69. Pokala N., Liu Q., Gordus A., Bargmann C. I. (2014) Inducible and titratable silencing of *Caenorhabditis elegans* neurons in vivo with histamine-gated chloride channels. *Proc Natl Acad Sci U S A* **111**:2770-2775 <https://doi.org/10.1073/pnas.1400615111> | PubMed
70. Itskovits E., Levine A., Cohen E., Zaslaver A. (2017) A multi-animal tracker for studying complex behaviors. *BMC biology* **15**:1-16 <https://doi.org/10.1186/s12915-017-0363-9> | PubMed
71. Lockery S. R., Lawton K. J., Doll J. C., Faumont S., Coulthard S. M., Thiele T. R., Chronis N., McCormick K. E., Goodman M. B., Pruitt B. L. (2008) Artificial dirt: microfluidic substrates for nematode neurobiology and behavior. *J Neurophysiol* **99**:3136-3143 <https://doi.org/10.1152/jn.91327.2007> | PubMed
72. De Boer E., Kuyper P. (1968) Triggered correlation. *IEEE Transactions on Biomedical Engineering* **169**:169-179 <https://doi.org/10.1109/tbme.1968.4502561> | PubMed
73. Bryant H. L., Segundo J. P. (1976) Spike initiation by transmembrane current: a white-noise analysis. *The Journal of physiology* **260**:279-314 <https://doi.org/10.1113/jphysiol.1976.sp011516> | PubMed

74. Davidson A. G., O'Dell R., Chan V., Schieber M. H. (2007) Comparing effects in spike-triggered averages of rectified EMG across different behaviors. *J Neurosci Methods* **163**:283-294 <https://doi.org/10.1016/j.jneumeth.2007.03.010> | PubMed
75. Ji N., Venkatachalam V., Rodgers H. D., Hung W., Kawano T., Clark C. M., Lim M., Alkema M. J., Zhen M., Samuel A. D. (2021) Corollary discharge promotes a sustained motor state in a neural circuit for navigation. *eLife* **10**:e68848 <https://doi.org/10.7554/eLife.68848> | PubMed
76. Riedl J., Fieseler C., Zimmer M. (2022) Tyraminergetic corollary discharge filters reafferent perception in a chemosensory neuron. *Curr Biol* **32**:3048-3058.e3046 <https://doi.org/10.1016/j.cub.2022.05.051> | PubMed
77. Ray A., Gordus A. (2025) Nonlinear integration of sensory inputs and behavioral state by a single neuron in *C. elegans*. *Curr Biol* **35**:5534-5548.e5534 <https://doi.org/10.1016/j.cub.2025.10.006> | PubMed
78. Bourgou S., Rahali F. Z., Ourghemmi I., Saidani Tounsi M. (2012) Changes of peel essential oil composition of four Tunisian citrus during fruit maturation. *ScientificWorldJournal* **2012**:528593 <https://doi.org/10.1100/2012/528593> | PubMed
79. Neelakandan P., Young C.-C., Hameed A., Wang Y.-N., Chen K.-N., Shen F.-T. (2021) Volatile 1-octanol of tea (*Camellia sinensis* L.) fuels cell division and indole-3-acetic acid production in phylloplane isolate *Pseudomonas* sp. NEEL19. *Scientific Reports* **11**:2788 <https://doi.org/10.1038/s41598-021-82442-7> | PubMed
80. Tsunozaki M., Chalasani S. H., Bargmann C. I. (2008) A behavioral switch: cGMP and PKC signaling in olfactory neurons reverses odor preference in *C. elegans*. *Neuron* **59**:959-971 <https://doi.org/10.1016/j.neuron.2008.07.038> | PubMed
81. Hukema R. K., Rademakers S., Dekkers M. P., Burghoorn J., Jansen G. (2006) Antagonistic sensory cues generate gustatory plasticity in *Caenorhabditis elegans*. *EMBO J* **25**:312-322 <https://doi.org/10.1038/sj.emboj.7600940> | PubMed
82. Jang H., Kim K., Neal S. J., Macosko E., Kim D., Butcher R. A., Zeiger D. M., Bargmann C. I., Sengupta P. (2012) Neuromodulatory state and sex specify alternative behaviors through antagonistic synaptic pathways in *C. elegans*. *Neuron* **75**:585-592 <https://doi.org/10.1016/j.neuron.2012.06.034> | PubMed
83. Murayama T., Maruyama I. N. (2013) Decision making in *C. elegans* chemotaxis to alkaline pH: Competition between two sensory neurons, ASEL and ASH. *communicative & integrative Biology* **6**:1007-1012 <https://doi.org/10.4161/cib.26633> | PubMed
84. Ghosh D. D., Sanders T., Hong S., McCurdy L. Y., Chase D. L., Cohen N., Koelle M. R., Nitabach M. N. (2016) Neural architecture of hunger-dependent multisensory decision making in *C. elegans*. *Neuron* **92**:1049-1062 <https://doi.org/10.1016/j.neuron.2016.10.030> | PubMed
85. Chalfie M., Sulston J. E., White J. G., Southgate E., Thomson J. N., Brenner S. (1985) The neural circuit for touch sensitivity in *Caenorhabditis elegans*. *Journal of Neuroscience* **5**:956-964 <https://doi.org/10.1523/jneurosci.05-04-00956.1985> | PubMed
86. Piggott B. J., Liu J., Feng Z., Wescott S. A., Xu X. S. (2011) The neural circuits and synaptic mechanisms underlying motor initiation in *C. elegans*. *Cell* **147**:922-933 <https://doi.org/10.1016/j.cell.2011.08.053> | PubMed
87. Grothe B., Pecka M., McAlpine D. (2010) Mechanisms of sound localization in mammals. *Physiological reviews* **90**:983-1012 <https://doi.org/10.1152/physrev.00026.2009> | PubMed
88. Witvliet D., Mulcahy B., Mitchell J. K., Meirovitch Y., Berger D. R., Wu Y., Liu Y., Koh W. X., Parvathala R., Holmyard D. (2021) Connectomes across development reveal principles of brain maturation. *Nature* **596**:257-261 <https://doi.org/10.1038/s41586-021-03778-8> | PubMed
89. Campbell J. C., Polan-Couillard L. F., Chin-Sang I. D., Bendena W. G. (2016) NPR-9, a galanin-like G-protein coupled receptor, and GLR-1 regulate interneuronal circuitry underlying multisensory integration of environmental cues in *Caenorhabditis elegans*. *PLoS genetics* **12**:e1006050 <https://doi.org/10.1371/journal.pgen.1006050> | PubMed

90. Summers P. J., Layne R. M., Ortega A. C., Harris G. P., Bamber B. A., Komuniecki R. W. (2015) Multiple sensory inputs are extensively integrated to modulate nociception in *C. elegans*. *Journal of Neuroscience* **35**:10331-10342 <https://doi.org/10.1523/jneurosci.0225-15.2015> | PubMed
91. Schindelin J., Arganda-Carreras I., Frise E., Kaynig V., Longair M., Pietzsch T., Preibisch S., Rueden C., Saalfeld S., Schmid B., *et al.* (2012) Fiji: an open-source platform for biological-image analysis. *Nat Methods* **9**:676-682 <https://doi.org/10.1038/nmeth.2019> | PubMed
92. Dubbs A., Guevara J., Yuste R. (2016) moco: Fast Motion Correction for Calcium Imaging. *Front Neuroinform* **10**:6 <https://doi.org/10.3389/fninf.2016.00006> | PubMed
93. Brenner S. (1974) The genetics of *Caenorhabditis elegans*. *Genetics* **77**:71-94 <https://doi.org/10.1093/genetics/77.1.71> | PubMed
94. Stiernagle T. (2006) Maintenance of *C. elegans*. *WormBook* <https://doi.org/10.1895/wormbook.1.101.1> | PubMed
95. Itskovits E., Ruach R., Kazakov A., Zaslaver A. (2018) Concerted pulsatile and graded neural dynamics enables efficient chemotaxis in *C. elegans*. *Nat Commun* **9**:2866 <https://doi.org/10.1038/s41467-018-05151-2> | PubMed
96. Yu X., Creamer M. S., Randi F., Sharma A. K., Linderman S. W., Leifer A. M. (2021) Fast deep neural correspondence for tracking and identifying neurons in *C. elegans* using semi-synthetic training. *eLife* **10** <https://doi.org/10.7554/elife.66410> | PubMed
97. Kuramochi M., Doi M. (2017) A Computational Model Based on Multi-Regional Calcium Imaging Represents the Spatio-Temporal Dynamics in a *Caenorhabditis elegans* Sensory Neuron. *PLoS One* **12**:e0168415 <https://doi.org/10.1371/journal.pone.0168415> | PubMed
98. Mahadevan A. S., Tooley U. A., Bertolero M. A., Mackey A. P., Bassett D. S. (2021) Evaluating the sensitivity of functional connectivity measures to motion artifact in resting-state fMRI data. *NeuroImage* **241**:118408 <https://doi.org/10.1016/j.neuroimage.2021.118408> | PubMed
99. Liégeois R., Santos A., Matta V., Van De Ville D., Sayed A. H. (2020) Revisiting correlation-based functional connectivity and its relationship with structural connectivity. *Network Neuroscience* **4**:1235-1251 [https://doi.org/10.1162/netn\\_a\\_00166](https://doi.org/10.1162/netn_a_00166) | PubMed
100. Myers L., Sirois M. J. (2004) Spearman correlation coefficients, differences between. *Encyclopedia of statistical sciences* **12** <https://doi.org/10.1002/0471667196.ess5050>

## Peer reviews

### Reviewer #1 (Public review):

The authors investigated the response of worms to the odorant 1-octanol (1-oct) using a combination of microfluidics-based behavioral analysis and whole-network calcium imaging. They hypothesized that 1-oct may be encoded through two simultaneous, opposing afferent pathways: a repulsive pathway driven by ASH, and an attractive pathway driven by AWC. And the ultimate chemotactic outcome is likely determined by the balance between these two pathways.

It is not surprising that 1-octanol is encoded as attractive at low concentrations and repulsive at higher concentrations. However, the novel aspect of this study is the discovery of the combinatorial coding of 1-oct in the periphery, where it serves as both an attractant and a repellent. Furthermore, the study uses this dual encoding as a model to explore the neural basis of sensory-driven behaviors at a whole-network scale in this organism. The basic conclusions of this study are well supported by the behavioral and imaging experiments, though there are certain aspects of the manuscript that would benefit from further clarification.

A key issue is that several previous studies have demonstrated a combinatorial and concentration-dependent coding of odorant sensing in the nematode peripheral nervous

system. Specifically, ASH and AWC are the primary receptors for repellent and attractive responses, respectively. However, other neurons such as AWB, AWA, and ADL are also involved in the coding process. These neurons likely communicate with different interneurons to contribute to 1-oct-induced outputs. The authors' conclusion that loss of *tax-4* reduces attractive responses and that *osm-9* mutants reduce repulsive responses is not entirely convincing. *TAX-4* is required for both AWC (an attractive neuron) and AWB (a repulsive neuron), and *osm-9* is essential for ASH, ADL, and AWA (attraction-associated). Therefore, the observed effects on the attractive and repulsive responses could be more complex. Additionally, the interpretation of results involving the use of IAA to reduce the contribution of AWC at lower concentrations lacks clarity.

The authors did not observe any increased correlation between motor command interneurons and sensory neurons, which is consistent with the absence of a consistent relationship between state transitions and 1-oct application. Furthermore, they did not observe significant entrainment of AIB activity with the 2.2 mM 1-oct application. This might be due to the animals being anesthetized with 1 mM tetramisole hydrochloride, which could affect neural activity and/or feedback from locomotion.

Comments on revisions:

The authors have addressed all my previously raised concerns.

<https://doi.org/10.7554/eLife.104828.2.sa3>

## Reviewer #2 (Public review):

Summary:

The authors used whole-network imaging to identify sensory neurons that responded to the repellent 1-octanol. While several olfactory neurons responded to the initial onset of odor pulses, two neurons consistently responded to all the pulses, ASH and AWC. ASH typically activates in response to repellants, and AWC typically activates in response to the removal of attractants. However in this case, AWC activated in response to the removal of 1-octanol, which was unexpected because 1-octanol is a harmful repellent to the worm. The authors further investigated this phenomenon by testing different concentrations of 1-octanol in a chemotaxis assay, and found that at lower (less harmful) concentrations the odor is actually an attractant, but becomes repulsive at higher concentrations. The amplitude of the ASH response appeared to be modulated by concentration, but this was not true for AWC. The authors propose a model where the behavioral response of the worm is the result of integrating these two opposing drives, where repulsion is a result of the increased ASH activity over-riding the positive drive from AWC. The authors further tested this theory by testing mutants that ablated the AWC response (*tax-4* or *AWC::HisCl*) or ASH response (*osm-9* or *ASH::HisCl*). The chemo-silencing (*HisCl*) and *tax-4* experiments were consistent with their hypothesis, while the *osm-9* mutation had a limited impact on chemotaxis behavior, highlighting the potential role of *osm-9*-independent signaling in ASH in response to 1-octanol. While the interneuron(s) that integrate these signals to influence behavior were not identified, the authors did find that increasing concentrations of 1-octanol did increase the likelihood of AVA activity, a neuron which drives reversals (and hence, behavioral repulsion).

Strengths:

This was simple and elegant work that identified specific neurons of interest which generated a hypothesis, which was further tested with mutants that altered neuronal activity. The authors performed both neuronal imaging and behavioral experiments to verify their claims.

Weaknesses:

The authors note that other sensory neurons likely contribute to 1-octanol chemotaxis. Given the NeuroPAL data, it would have been nice to identify these other neurons as well. However, the reviewer is aware that this is tangential to the primary focus of this study.

<https://doi.org/10.7554/eLife.104828.2.sa2>

### Reviewer #3 (Public review):

Summary:

This work describes how two chemosensory neurons in *C. elegans* drive opposite behaviors in response to a volatile cue. Because they have different concentration dependencies, this leads to different behavioral responses (attraction at low concentration and repulsion at high concentration). It has been known that many odorants that are attractive at low concentrations are aversive at high concentrations, and the implicated neurons (at least AWC for attraction and ASH for repulsion) have been well established. None the less, by studying behavior and neural responses in a common context (odor pulses, as opposed to gradients) this provides a clear picture of how these sensory neurons may guide the dose dependent response by separately modulating odor entry and odor exit behaviors.

Strengths:

(1) This work provides good evidence that worms are attracted to low concentrations and repelled by high concentrations of 1-oct. Calcium imaging also makes it clear that dose-dependence of this response is stronger for ASH than AWC.

(2) This work presents calcium imaging and behavior with the same stimulus (sudden pulses in volatile odor concentration), while previous studies often focus on using neuronal responses to pulses to understand navigation of gentle gradients.

Weaknesses:

(1) As a whole it is not clear precisely how important AWC is (compared to other cells) for the attractive response (as the authors correctly acknowledge).

(2) The evidence that AIB minus AVA contains relevant information is weak. It appears the entrainment index in Fig. 6H for AIB-AVA could easily be explained by the negative entrainment between AVA and the stimulus (along with no effect or role for AIB). This is suggested by the similar p-values and similar distribution of random EIs (stretched and mirrored) between the first and last rows of this figure.

(3) The model in Figure 7 would be strengthened if it was demonstrated that IAA is attractive when worms are saturated in a  $1/10^4$  concentration. Panel 7G (and ref. 39) indicate that  $10^{-4}$  IAA activates ASH, which would suggest a different explanation for the change from attraction to repulsion in 7C.

<https://doi.org/10.7554/eLife.104828.2.sa1>

### Author response:

The following is the authors' response to the original reviews.

**Public Reviews:**

**Reviewer #1 (Public review):**

*...other neurons such as AWB, AWA, and ADL are also involved in the coding process. These neurons likely communicate with different interneurons to contribute to 1-octinduced outputs. The authors' conclusion that loss of tax-4 reduces attractive responses and that osm-9 mutants reduce repulsive responses is not entirely convincing. TAX-4 is required for both AWC (an attractive neuron) and AWB (a repulsive neuron), and osm-9 is essential for ASH, ADL, and AWA (attraction-associated). Therefore, the observed effects on the attractive and repulsive responses could be more complex. Additionally, the interpretation of results involving the use of IAA to reduce the contribution of AWC at lower concentrations lacks clarity. A more effective approach might involve using transgenically expressed miniSOG or histamine (HisCl1) to specifically inhibit AWC neurons.*

We agree that the sensory inputs into chemotactic behavior are likely more complex, involving other neurons besides ASH and AWC. We now explicitly discuss possibility in the Discussion (lines 449-467).

We have also utilized transgenically expressed HisCl1 in ASH and AWC to address this concern. Crucially, we observe that some of the effects of the broad mutations are reproduced by inactivating ASH and AWC. This finding validates our overall hypothesis that sensory-driven behavior is a balance of simultaneous afferent inputs of opposite valence AND shows that ASH and AWC are involved as expected. We are currently performing a comprehensive analysis of sensory inputs into locomotory decision making, including the neurons mentioned in the Reviewer's comment.

We also agree that using IAA is not a very clean way to inactivate AWC. The AWC HisCl results referenced above should alleviate this concern. However, the IAA result does put our findings into a broader context of multi-sensory integration which demonstrates the potential usefulness and selective advantages of the dual-input coding architecture that we are hypothesizing.

*Furthermore, they did not observe significant entrainment of AIB activity with the 2.2 mM 1-oct application. This might be due to the animals being anesthetized with 1 mM tetramisole hydrochloride, which could affect neural activity and/or feedback from locomotion.*

We now mention these caveats "It is possible that immobilization and anesthetization may be affecting AIB responses to sensory activity and/or proprioceptive feedback from locomotion. However, it is also possible that motor feedback from RIM was obscuring the sensory signal." Line 357

*It is unclear whether subtracting AVA activity from AIB activity provides a valid measure. Similarly, it is unclear how the behavioral data from freely moving worms compares to the whole-network calcium imaging results obtained from immobilized worms.*

Ray and Gordus 2025 (Current Biology 35:5534) recently demonstrated that AIB activity can be modeled as the additive convolution of AVA, AWC, and AIA activity, lending validity to our subtractive approach. In their study, AVA was the major contributor, but addition of AWC and AIA signals (i.e. sensory inputs) resulted in a significant greater accuracy. We have now mentioned their work in the manuscript (line 363) "To address this possibility, we subtracted AVA activity, representing the motor state, from the AIB activity (AVA closely mirrors RIM), based on the observation that AIB activity can be modeled as the sum of convolutions of motor activity and sensory activity." (lines 360-363)

The relationship between network activity in freely moving worms and immobilized worms has been explored by Kato et al 2015 (Cell 163:656-669); we now refer to this work on line 131 "These transitions are related to network state changes which drive spontaneous reversals

during foraging in freely moving worms. Immobilization and anesthetization, necessary for confocal imaging, distort certain aspects of these motor command sequences compared to freely moving worms executing the motor commands and receiving proprioceptive feedback. However, the intrinsic motor programs remain intact under these conditions.” (lines 131-136)

**Reviewer #2 (Public review):**

*tax-4, but not osm-9 mutants were used in chemotaxis and imaging assays. It would have been nice to have osm-9 results as well for these assays. The mutants are not specific to AWC and ASH. Cell-specific rescue of these neurons would have strengthened the proposed model.*

Osm-9 data are now included in the chemotaxis assays (Fig. 4E).

Cell-specific HisCl data are now included for ASH and AWC (Fig. 4F, G, 5D), confirming our proposed model.

Limited *tax-4* data were included in the imaging (Fig. 6), but unfortunately, NeuroPAL imaging in *tax-4* has proven to be technically difficult. NeuroPAL images in the *tax-4* background appear different, perhaps because of developmental effects on gene expression due to the lack of sensory input (recall that the NeuroPAL color scheme is based on the relative expression levels of 40+ neuronal promoters). Inactivation of individual sensory neurons using HisCl1 or other transgenes may be the simpler approach.

The Results and Discussion have been significantly rewritten to incorporate these new data

We are currently working on a comprehensive study of the sensory inputs into locomotory decision making in the context of chemosensation, which we expect to reveal roles of other neurons besides ASH and AWC and provide a fuller picture of the complexities of this system.

**Reviewer #3 (Public review):**

*(1) It is not clear precisely how important AWC is (compared to other cells) for the attractive response, though the presence of odor-off behavior implicates it. This could be resolved by looking at additional mutants (tax-4 is broad).*

We have addressed this concern using transgenically-expressed HisCl1 which has demonstrated a clear role for AWC in overall chemotaxis and locomotory decision making upon encountering the 1-oct/buffer interface in microfluidics devices (Fig. 4F, G, 5D).

*(2) Relatedly, dose-dependent chemotaxis data (Figure 4C, D) should be provided for osm-9 animals to get a sense of the degree to which dose-dependence is explained by ASH.*

Osm-9 data now included (Fig. 4E)

The Results and Discussion have been significantly rewritten to incorporate these new data

*(3) Figure 4A, B should include average traces with errors, as there are several ways the responses can vary across conditions.*

Averaged traces with error bars now shown (Fig. 4A, B)

*(4) The data in Figure 6G does not appear to have error bars.*

Error bars now shown for 6G

*Also, it would help to include a more conventional demonstration of AIB responding to stimuli (e.g. averaging stimulus-aligned responses as a percent of the fluorescence value*

| *at stimulus onset to perform the desired subtraction).*

Fig. 6G top panel shows the stimulus-aligned responses of AIB with no subtraction performed. The 6 sequential stimulations are shown as a single continuous trace, consistent with the experimental protocol utilized. Averaging was performed across the 12 individuals of the sample set. However, we did not calculate the average of responses within a dataset (i.e. first plus second plus third etc.) to avoid obscuring any sensitization/desensitization that might be occurring with multiple stimuli.

| *Subtracted calcium traces are harder to interpret. As it stands, the evidence that sensory signals are persisting in AIB and not being shunted by proprioceptive feedback in microfluidic devices is not strong.*

Addressing the point about proprioceptive feedback in microfluidics devices, the following sentence was added in the Results section: “Immobilization distorts certain aspects of these motor command sequences compared to freely moving worms executing the motor commands and receiving proprioceptive feedback, but the intrinsic motor programs remain intact.” (lines 131-136).

To add context for the AIB-AVA subtraction, Ray and Gordus 2025 (Current Biology 35:5534) recently demonstrated that AIB activity can be modeled as the additive convolution of AVA, AWC, and AIA activity, lending validity to our subtractive approach. In their study, AVA was the major contributor, but addition of AWC and AIA signals (i.e. sensory inputs) resulted in a significant greater accuracy. We have now mentioned their work in the manuscript: “To address this possibility, we subtracted AVA activity, representing the motor state, from the AIB activity (AVA closely mirrors RIM), based on the observation that AIB activity can be modeled as the sum of convolutions of motor activity and sensory activity.” (lines 360-363)

| **Recommendations for the authors:**

| **Reviewer #1 (Recommendations for the authors):**

| *Figure 1: The number of replicates (n) is missing.*

In Fig. 1D, only a single trial is shown as a representative example rather than averages, which would necessitate error bars. The Results and Figure Legend text has been updated to clarify this, and the average CI is now included in the first Results section (lines 111, 976)

| *Figure 4: The sample size (n = 3-5) is relatively small, which may limit the statistical power.*

Sample size was increased to 5 for all data points shown on the new graph (Fig. 4E and noted in the figure legend (line 1019)

| *Figure 4: The 0.22 mM concentration significantly affects both AWC and ASH. It is also unclear whether this concentration also affects other neurons, such as AWB, ADL, and AWA.*

We have not performed exhaustive analysis of other neurons in these datasets. These analyses are difficult and time consuming, so we have opted to present a dataset which supports our hypothesis that multiple afferent pathways of opposite valence act in a balanced way to drive chemotaxis. We are currently performing an in-depth analysis of the sensory inputs into the circuit, which we expect to present in a future study


| **Reviewer #2 (Recommendations for the authors):**

| *The tax-4 and osm-9 experiments are great, but I recommend clarifying that tax-4 and osm-9 are expressed in other neurons as well. The text gives the impression that these*

*mutants are specific to AWC and ASH, respectively. The authors should note these caveats.*

This concern is thoroughly addressed in the descriptions and rationale presented for the use of ASH and AWC HisCl strains.

*The authors should also provide the code used to interpret their results.*

Code will be provided through [Zenodo.org](https://zenodo.org) 

**Reviewer #3 (Recommendations for the authors):**

*It would help to clarify (early on) the degree to which you are attributing responses to particular cells (e.g. AWC) as opposed to a class of cells with AWC as an example.*

This concern is thoroughly addressed in the descriptions and rationale presented for the use of ASH and AWC HisCl strains.

*The NeuroPAL imaging and analysis (especially Figures 3D, E) is a bit distracting and appears non-essential. If possible, it would help to combine Figures 2 and 3 with a focus on panels 3ABC to streamline the narrative.*

We would prefer to keep the present format so the reader can appreciate the power of the whole-brain approach for analyzing network activity and behavioral outputs in the context of sensory-motor responses. Specifically, our insight that attractive and aversive afferent inputs were activated simultaneously was wholly dependent on this approach. Otherwise, there would have been little to no reason for examining AWC activity at aversive 1-oct concentrations, which was essentially the foundation of the study.

To highlight this point, we have added the following sentence in the Discussion: “This novel insight highlights the value of the whole-brain approach (enabled by the NeuroPAL system) for studying the network dynamics underlying sensory driven behaviors.” Lines 431-433.

<https://doi.org/10.7554/eLife.104828.2.sa0>